Lawrence Berkeley Laboratory
UNIVERSITY OF CALIFORNIA

Materials & Molecular Research Division

RADIAL DISTRIBUTION FUNCTION AS AN ANALYSIS TECHNIQUE

A.W. Pearson
(M.S. Thesis)

May 1984

Prepared for the U.S. Department of Energy under Contract DE-AC03-76SF00098

DISCLAIMER

LBL-16604

RADIAL DISTRIBUTION FUNCTION AS AN ANALYSIS TECHNIQUE

Anthony W. Pearson

(M.S. Thesis)

Materials and Molecular Research Division
Lawrence Berkeley Laboratory
University of California
Berkeley, CA 94720

RADIAL DISTRIBUTION FUNCTION AS AN ANALYSIS TECHNIQUE

Anthony W. Pearson
(M.S. Thesis)

Materials and Molecular Research Division
Lawrence Berkeley Laboratory
University of California
Berkeley, CA 94720

ABSTRACT

Diffraction patterns for Cu as found in a perfect FCC lattice were generated for various particle sizes and shapes using a computer model based on the Debye-Sum. These patterns were Fourier transformed to yield the "radial distribution function" $G(R) = 4\pi R(\rho(R)-\rho_0)$. This function was studied in relation to five variables, i.e., 1) particle size, 2) particle shape, 3) scattering vector termination, 4) the influence of small angle scattering due to sample size and, 5) effect of vibrational atomic displacements. Particle sizes of up to 30Å were found to influence G(R) as related to determination of the first coordination shell. The effect of volume scattering was to displace the G(R) curve negatively, but neither peak position nor area were affected. The measurement of ρ_0 was affected and the effective ρ_0 present with SAXS removed must be taken into account when calculating coordination shells.

ACKNOWLEDGEMENT

My gratitude and thanks are extended to all of those people whose time and affection have been invested in my pursuit of this work. Especially to Elizabeth for many lost weekends and her tolerance of neglect. To Professor Bragg, special thanks are given for providing many insightful ideas and time for discussions as well as my financial support for the length of my stay at the University. Thanks are also extended to him for having a deep concern about all aspects of my course study at the University. Thanks also go to Professor Gronsky for his support and confidence as well as patience. I must also pay sincere thanks to all of those people who in my life have taught me how to solve problems from not only an analytic foundation, but with an inquisitive, questioning viewpoint. These gifts have been given to me most unselfishly and although this work may not be reflective of this in any profound sense, I hope that it shows that I have not been wholly neglectful of these philosophies.

This work was supported by the Director, Division of Material Sciences, Office of Basic Energy Sciences of the U.S. Department of Energy under Contract No. DE-AC03-76SF00098.

TABLE OF CONTENTS

INTRODUCTION

This study was originated in conjunction with studies of glassy carbon in the hopes that it might be possible to obtain high resolution information regarding the turbostatic stacking nature of the material, and whether any presence of hydrogen in between stacking layers could be detected. This problem raised many other fundamental questions about the "Radial Distribution Function" (RDF) such as: 1) effect of small-angle-scattering (SAXS). 2) effect of particle size. 3) effect of particle shape. 4) experimental termination error. 5) temperature correction. The main emphasis of this work was to ascertain the effect of particle size upon the RDF and to discover at approximately what particle size the first three coordination shells would be fully developed as determined by RDF analysis.

Related Carbon studies have been performed by Ergun,[3] Pings,[21] and Lindberg.[22] These papers dealt with the structural nature of Glassy Carbon and not with the analytical nature of the RDF.

Papers pertaining directly to the analytical nature of the RDF have been widely published. Direct examples are: "Influence of Neglected Small-Angle Scattering in Radial Distribution Function Analysis", Cargill,[1]. "Analysis of Termination Effects on Atomic Radial Density Curves," Ergun[2] et al. Discussion of the dependence of the "Correlation Function" on the scattering volume is discussed by Debye[4] and the dependence of the RDF on shape is discussed by Riley.[5] Other related papers have been published by Diamond,[23] Franklin,[24] and Suzuki.[25]

TECHNICAL DISCUSSION

Computer Hardware

All data were produced on a Control Data Corporation 7600 series mainframe computer. This machine utilizes a 60-bit pipelined architecture with a small-core memory access time of 275 Nanoseconds. The processing architecture consists of a main central processing unit (CPU) and eight peripheral processing units (PPU). These units are tightly synchronized in time. Instructions in all but one of the units are processed with every clock cycle; hence, the term "pipeline" architecture. The number of raw multiplications and divisions possible is about 2.4×10^6 multiplications and about 9.0×10^5 divisions. These numbers are arrived at by taking the reciprocal of the product of clock period and the number of periods per operation. The CDC-7600 utilizes a 27.5 Nanosecond clock and 3-instruction codes to perform a multiply and 2-instruction codes to perform a divide. Assuming an instruction is executed every clock-cycle the details are worked as follows:

$$(\text{Multiplications/Seconds}) = \sum_{m=1}^{3} IC_m \, CP^{-1} = 2.42 \times 10^6$$

$$(\text{Divisions/Seconds}) = \sum_{m=1}^{2} IDC_m \, CP^{-1} = 9.09 \times 10^5$$

where: CP = 27.5 nanosecond clock period.

IC_m = # of clock periods utilized for instruction (m) in multiplication unit. (IC_m = 5 periods; for all m)

IDC_m = # of clock periods utilized for instruction (m) in division unit. (IDC_m = 20 periods; for all m)

Computer Software

The language utilized to produce the data was the CDC version of ANSI standard Fortran IV i.e., (FTN-4). This CDC compiler has several levels of optimizaton depending on whether the user is striving for faster execution time or faster compilation time. A program such as the one described for this project is extremeley CPU-bound and requires as much optimization of the code as is possible to speed execution time. For this reason the compiler was directed to produce object code at its highest level of optimization through the use of a control card option directive. Even using a compiler such as this at its highest level of optimization is inadequate and it is necessary to include a "vectored array" access scheme. See Appendix A for an example. Other optimization techniques such as reversal of summation, normalization of variables, and conversion of division to multiplication were used and are described in Appendix A.

A problem such as this is termed CPU-bound because the time involved for numerical calculation far exceeds the time utilized for I/O processes such as disk access or read and write operations. The majority of CPU time is used in performing the iterations of the quantity [Sin(KR)] and the square root function used in the distance

formula. These functions are the limiting factors because they need to be performed by high-level software routines. In comparison assembly language opcodes which perform floating point (adds, subtracts, divides and multiplies) all within hardware units in the machine, are orders of magnitude faster. The typical execution speed of an optimized floating point routine for SIN(X) is 24 μS as stated by Cassola.[8] Thus, computation of one value of SIN(X) must be considered as approximately 100 times slower than the accessing of variables from memory and illustrates this calculation as being the limiting factor in program execution speed.

The programs written utilize the Least-Squares-Polynominal Regression and Polynomial interpolation subroutines: (POLFIT, PVALUE) from the Sandia mathematical library version 7.2 of Lawrence Berkeley Laboratory. These subroutines were used to fit and interpolate a least-squares polynomial for the scattering factor f(k) to data found in the International Tables for X-Ray Crystallography, Vol III, the values were not corrected for dispersion. The polynomial fit found was excellent with a root-mean square error of less than 3 percent from point to point. The integration routine for G(R) was done using Simpson's 1/3 rule. The routine is specific for problems dealing with equal intervals, although the technique may be adapted for problems with unequal intervals. Simpson's 1/3 rule is used with an even number of intervals and has a global error of h^4, see Gerald.[15] This error is insignificant when small intervals are chosen for integrations.

METHODS OF COMPUTATION

Various methods of producing X-ray diffraction profiles by computational numerical method have been explored. One of the most general powder pattern methods uses a Lorentz or Gaussian profile equation integrated for all (hkl) reflections in reciprocal space and multiplied by the appropriate structure factor for the material (see H. Fichtner et al.).[6] This type of method is excellent for determining peak positions, shapes, relative intensities, and for answering questions concerning particle size, and strain since the method is easily adjusted to account for such variables. This method is also distinguished by its relative ease of being programmed in a high-level language such as Fortran IV, and its low CPU cost. However, this method must be rejected when questions of calculating the Radial Distribution Function are considered. The reason this method should not be used in calculating RDF is that intensities are not produced in "Electron Units." The transform kernel of the RDF consists of a delicate comparison between the scattering per atom in the ensemble being studied versus the scattering factor of a single atom. Due to this reason any failure in correcting either experimental or computational intensity data to Absolute Electron Units will result in wildly oscillating behavior of the transform [see (Klug and Alexander)[7] and Kaplow].[14]

Since the behavior of the RDF is critically dependent on data being in electron units the only solution to the problems posed other than pursuing theoretical answers was to use a Debye Summation. The

Debye Sum will yield perfectly adequate results for crystalline powder patterns, except that interparticle effects which give rise to a smoothing of small-angle scattering will be absent. The absence of this effect is due to the fact that the Debye sum is treating all scattering problems as an homogenous ideal gas composed of particles of a singular shape and size with no particle interactions (hence the gas is ideal). In crystalline powder patterns it's these interparticle interactions which give rise to smooth low-angle intensity data (see Riley[5]).

It's certainly conceivable to think of modifying the computational program using a Debye summation to not only account for these interactions, but to also include the result from having a distribution of particle sizes and shapes.

The main drawback of using a Debye sum calculation is the reason of feasibility. Considering a cube of side length Na; N=1,2,3 etc. the number of interactions which must be considered in a conventional Debye summation for an FCC lattice is $16N^6$ calculations. Obvious symmetry will reduce the problem to $4N^3$ $(2N^3-1)$ calculations, but reductions beyond this point involve producing an increasingly complex computer program and require a certain knowledge of matrice representation of crystal symmetry.[19] Three (3) programs have been successfully produced with the following characteristics:

(1) Vectored Loop Method: Using vectored looping techniques the Debye sum is calculated for an FCC lattice using $4N^3(2N^3-1)$ calculations for all N. This method has an N^6 relation.

(2) Z-Stacking Method: Using vectored looping techniques the Debye sum is calculated for an FCC lattice using $(N-1)\ (1 + 8N^4)-8N^3$ calculations for all N. This method has an N^5 relation for large N.

(3) Array Symmetry Method: Using a qualitative symmetry found by inspection; the Debye sum is calculated for an FCC lattice using approximately N^2 calculations. It's suspected that the program has a flaw which prevents it from functioning for all N.

In this paper intensities were calculated using the Debye sum expressed as follow:

$$I.E.U(K) = 4N^3 f^2(K) + 2f^2(K) \sum_{I=1}^{4N^3-1} \sum_{J=I}^{4N^3} \frac{\mathrm{Sin}(KR_{IJ})}{KR_{IJ}} \qquad (1)$$

where:

$K = 4\pi \mathrm{Sin}(\theta)/\lambda$; the scattering vector

I.E.U.(K) = intensity in absolute electron units.

f(K) = scattering factor of the atom being studied.

R_{IJ} = the absolute magnitude of the distance between the atom I and the atom J in the ensemble under study.

The computational procedure for I.E.U.(K) is as follows:

1) The shape of the particle is decided upon and the algorithm for that shape is placed in the program so as to create atoms at the desired real-space coordinates. The particle shapes used for this problem were the cube, plate, and rod. Conservation of scattering volume was observed for all of these cases so that for any N value

implemented the results are comparable for any shape produced. The following shapes have the following structures:

Shape: Structure

Cube: The total number of atoms is $4N^3$ in accordance with an F.C.C. structure of length Na on a side. The cube has N unit cells per degree of freedom and is thus an equiaxed structure.

Plate: The total number of atoms is $4N^3$. The plate structure is one (1) unit cell thick in the [001] direction; N unit cells wide in the [010] direction, and N^2 unit cells long in the [100] direction.

Rod: The total number of atoms is $4N^3$. The rod structure is one (1) unit cell thick in the [001] direction and in the [010] direction. The rod is N^3 unit cells long in the [100] direction.

2) The coordinates of the structure are arranged in conventional F.C.C. fashion using the standard translation formula of: X_n,Y_n,Z_n; $X_n+1/2$, $Y_n+1/2$, Z_n; $X_n+1/2,Y_n,Z_n+1/2$; $X_n,Y_n+1/2$, $Z_n+1/2$ for $n = 1,2...N^3$. The placement of the coordinates X_n,Y_n,Z_n are determined by the shape of the particle as per the criteria previously explained. All of these coordinates are placed in memory.

3) The intensities may now be generated directly from the Debye sum using any of the three programming techniques previously discussed. I.E. the Z-stacking method, vectored loop method, or array symmetry method.

Vectored Loop Method

Using vectored loops shown in Appendix A the summation is done as shown in Equation 1 to arrive at I.E.U.(K).

Z-Stacking Method

The same set of transformations and vectored looping shown in Appendix A are used in this method, except the summation is performed with a multiplicity factor which reduces the number of terms needed for the summation. The number of terms is effectively reduced by (1/N). The method is accomplished as follows:

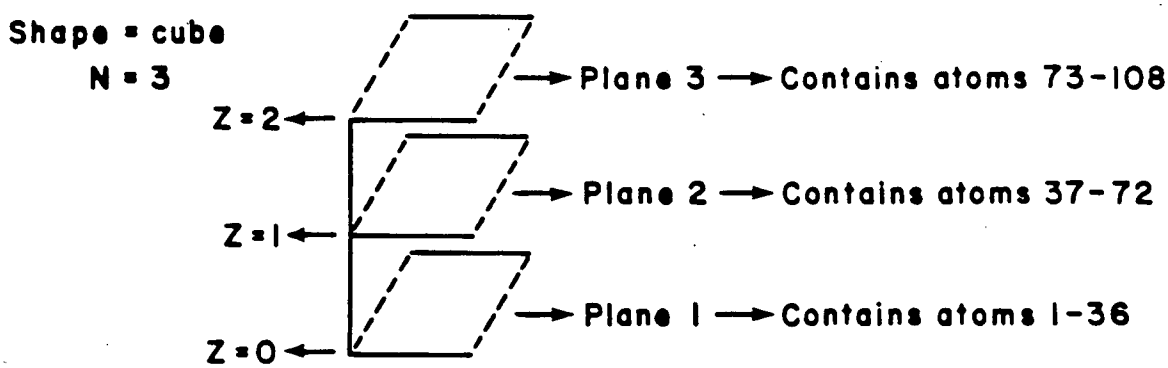

Figure A

Each plane shown in Figure A has $4N^2$ atoms or 36 atoms for the case above. As shown, each plane contains the atoms numbered in the scheme shown above and the summation may be reduced as follows:

$$\frac{I.E.U.(K)}{f^2(K)} = 4N^3 + 2N \sum_{I=1}^{4N^2-1} \sum_{J=I+1}^{4N^2} \frac{\sin(KR_{IJ})}{KR_{IJ}}$$

$$+ 2(N-1) \sum_{I=1}^{4N^2} \sum_{J=4N^2+1}^{8N^2} \frac{\sin(KR_{IJ})}{KR_{IJ}} \cdots 2 \sum_{I=1}^{4N^2} \sum_{J=4N^2(N-1)+1}^{4N^3} \frac{\sin(KR_{IJ})}{KR_{IJ}} \qquad (2)$$

This summation can be programmed without great difficulty.

Array Symmetry Method

This method is the most difficult to program but affords the greatest reduction in computational analysis. This method is arrived at by the analysis of the real-space interatomic distance matrix as follows:

1) First form the upper triangular matrix R with any element

$$R_{IJ} = \left[(X(I)-X(J))^2+(Y(I)-Y(J))^2+(Z(I)-Z(J))^2\right]^{1/2}$$

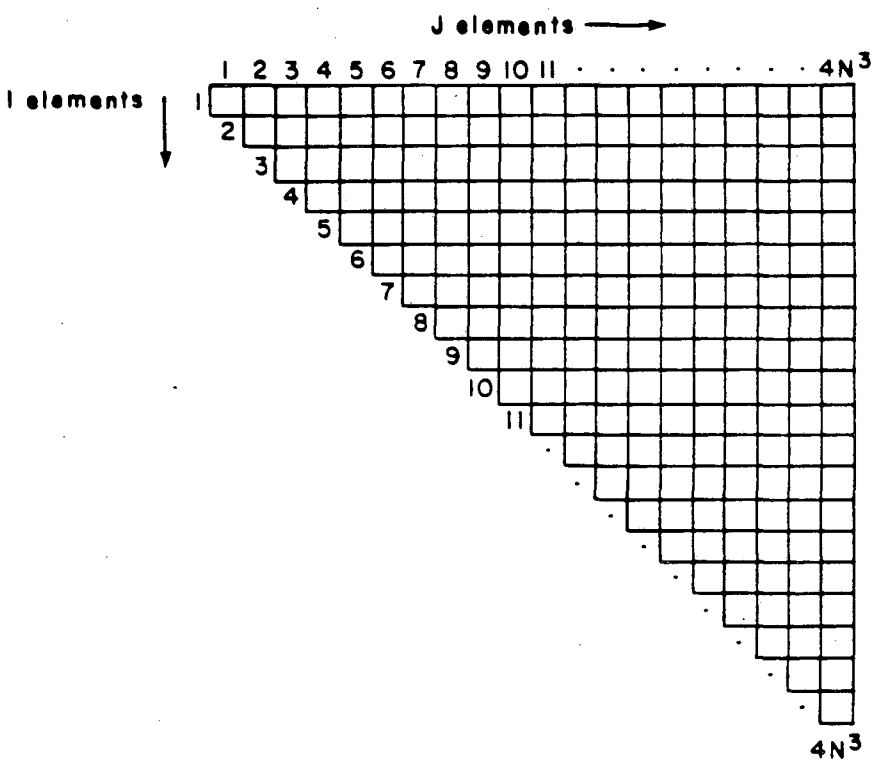

This matrix may be broken into 4x4 submatrices; but it's convenient to first perform the subtraction of all submatrices involving interactions of atoms within each individual unit cell. The contributions from these submatrices are easily analyzed.

The submatrices subtracted are of the form

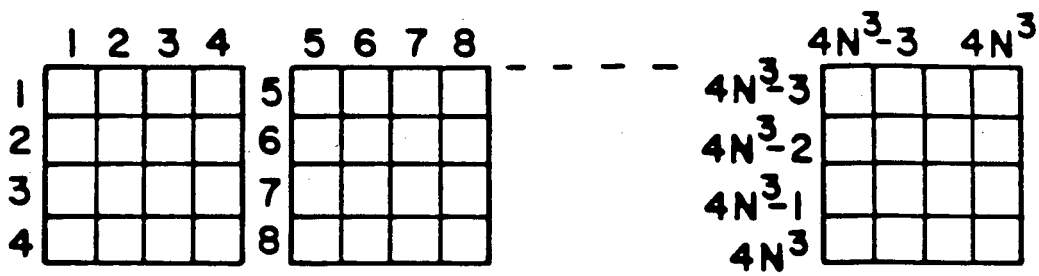

where $R_{12} = \frac{a}{\sqrt{2}} = R_{21} = R_{13} = R_{31} \cdots R_{41}$

where a = lattice constant for C_U = 3.6148Å. This subtraction leaves the upper triangular matrice in the following form

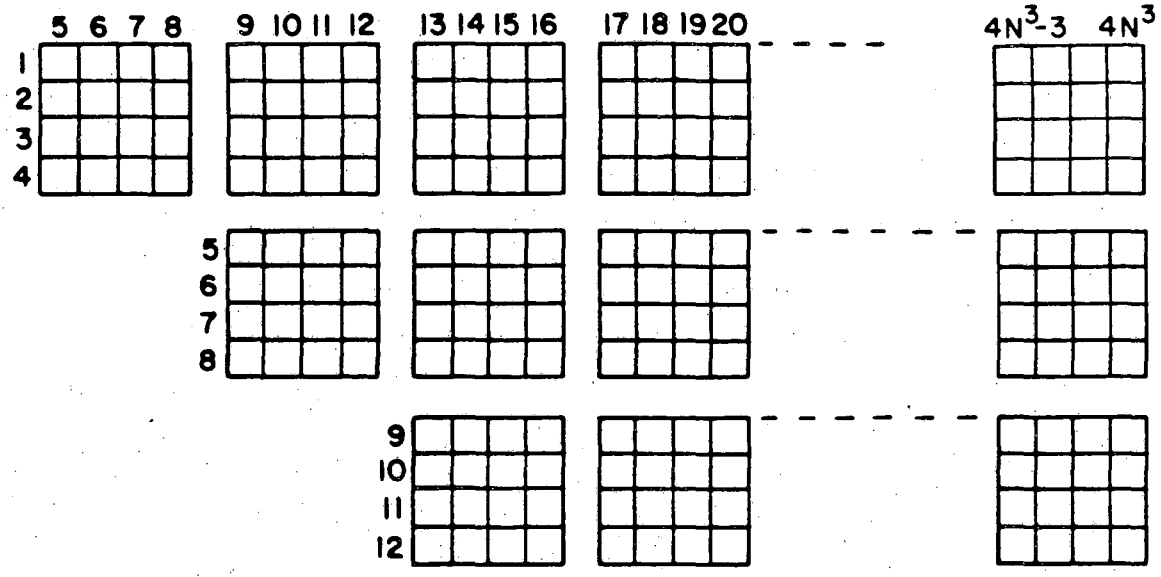

Examining a typical one of these submatrices reveals a symmetry pattern shown below:

	5	6	7	8
1	2	5	5	3
2	1	2	3	1
3	1	3	2	1
4	3	5	5	2

Note: the elements have been normalized by multiplying by $\sqrt{2}/a$ and squaring the result. Thus, a value of 1 for an element would represent an interatomic distance of $a/\sqrt{2}$ and a value of 2 would represent a distance of (a) etc.

The symmetry of each individual submatrice can be seen to involve the diagnoal terms and off-diagonal terms such that all the diagonal terms are equal, and the trace of the matrix is four (4) times the first element. All off-diagonal terms will be odd numbers if the diagonal elements are even and all diagonal elements must of necessity be even numbers.* Further symmetry can be found by comparing the sum of the off-diagonal elements below the diagonal to the sum of the off-diagonal elements above the diagonal and noting their equivalence. One other important symmetry that is observed is that any set of sub-matrices defined by having the same first element will also be such that the sum of the elements in any matrice of the set will be equal to the sum of the elements from any other matrice in the set. These symmetries by themselves are practically enough to define the whole problem analytically, the only symmetry factor which appears difficult to deduce is the repetition factor of each submatrice. The repetition factor would give the number of matrices contained in the set of all matrices with equal traces.

---

* All diagonal elements involve the distance between equivalent atoms in different unit cells. Since the atoms are equivalent the sum of the difference in their vector components will always add to a whole number, eg. $R_{15} = 1a$; $R_{59} = 2a$; $R_{1,29} = 3a$ such that any $(X_{diag} - X_{diag}) = 0,1,2,3...$etc.

This relation is also true for Y and Z vector components of any diagonal elements. Since the above relation is true it's true that all normalized diagonal components will be even whole numbers.

These symmetries however suggest a shorthand computational method involving the determinaton of the repetition factor. The program operates by generating all first diagonal elements except those of the type R_{IJ} where I = J and R_{IJ} where I > J and storing them in large core memory.

The program then stores the unique values of each first element such that a table will be formed which contains the value of each unique interatomic distance associated with a diagonal element. The program then finds the repetition factor of each element in the table by counting its redundancy from the table of all elements found in large core memory. Once the repetition factor of each element is found the program recreates the submatrix associated with each unique diagonal element. The Debye sum is then computed for each submatrix and multiplied by the repetition factor to yield the end result.

RADIAL DISTRIBUTION FUNCTION

The intensity distribution of coherent radiation from an ensemble of atomic scatterers was described by the Debye sum. The sum was computed by one of several methods described and produced an intensity pattern with the following five variables:

1) Vector termination point
2) Small angle scattering
3) Temperature diffuse scattering
4) Ensemble shape
5) Ensemble size

The first three (3) of these variables and their influence upon the radial distribution function have been treated in detail. However, the last two variables appear to not have been given as detailed an examination. Specifically variable (4) was given treatment by Riley,[5] and a treatment of variable (5) was not found, even though extensive treatments of particle size upon intensity distributions have been performed by such people as (Stokes and Wilson).[9] Each of these variables have been examined and the results are presented in the proceeding sections.

Radial Distribution Function Defined

The following treatment has been taken from Kaplow,[10] and (Enderby and Howells).[11]

G(R) is most frequently found in the form:

$$G(R) = 4\pi R(\rho(R)-\rho_0)$$

where

ρ_0 = average number of atoms per unit volume

$4\pi R^2\rho(R)dR$ = average number of atoms in a spherical shell a distance R from the center of an average atom; with the shell having thickness dR.

G(R) is related directly to the interference function through a Fourier sine inversion; and this is the property which makes it the most convenient function to use when transforming X-Ray intensity data. G(R) also appears when expressing potential energy equations such as the (PY) Percus Yevick model or the (HNC) Hyper-netted-Chain equation as expressed by Stell.[13] The appearance of G(R) in correlation functions such as the "direct correlation function" is also related to the properties of G(R) and its definition. The intention here is not to describe G(R) in terms of its atomic correlation functions or the existing atomic energy potentials of the system being studied. Rather that knowing an adequate expression for the interference function we wish to study the resulting G(R) by varying certain parameters in the interference function. G(R) may be expressed in terms of the Debye sum as follows:

$$G(R') = \frac{2}{\pi}\int_0^{\infty} K \sum_{I=1}^{4N^3} \sum_{J=I+1}^{4N^3} \frac{\mathrm{Sin}(KR_{IJ})}{KR_{IJ}} \mathrm{Sin}(KR')\, dK \qquad (3)$$

where R' = a continuous variable distinguished from R_{IJ}. This equation may be arrived at by substituting eq. 1 into the intensity kernel of the Zernicke-Prins equation given by eq. 4.

$$4\pi R^2\rho(R) = 4\pi R^2\rho_o + \frac{2R}{\pi}\int_0^\infty Ki(K)Sin(RK)dK \qquad (4)$$

where $Ki(K) = K\left[\frac{I.E.U(K)}{4N^3f^2(K)} - f^2(K)\right]$

Equation 4 may be easily rearranged to yield G(R) and the Fourier inversion relationship is easily visible in equation 5 and 6.

$$G(R) = 4\pi R(\rho(R)-\rho_o) = \frac{2}{\pi}\int_0^\infty Ki(K)Sin(RK)dK \qquad (5)$$

$$F(K) = Ki(K) = \int_0^\infty G(R)\ Sin(RK)dR \qquad (6)$$

Note the function G(R) depicted is purposely written in large capital script so as not to confuse it with the function little g(R) which is also similar to G(R) by the following relation:

$$g(R) = \frac{G(R)}{4\pi R\rho_o} + 1 \qquad (7)$$

The function little g(R) is the function which appears directly in potential energy expressions such as the PY and HNC equations.

RADIAL DISTRIBUTION FUNCTION AND VECTOR TERMINATION ERROR

The following treatment is adopted from Ergun.[2] The treatment is based on rewriting the Debye sum as a sum over all unique atomic distances and substituting it into the transform for G(R). Using the interference function (eq. 6) obtained from the Debye sum where the Debye sum has been corrected for vibration gives:

$$F(K) = K \sum_J \bar{m}_J \frac{\mathrm{Sin}(KR_J)_J e^{-K^2\delta_J^2}}{(KR_J)} \qquad (8)$$

where

$$K = \frac{4\pi \mathrm{Sin}(\theta)}{\lambda}$$

$\bar{m}_J$ = average number of interatomic distances R_J per atom in the ensemble.

δ_J^2 = mean square deviation in R_J due to vibration

R_J = a unique interatomic distance in the ensemble.

Note, the sum excludes the distance $R_J = 0$; and counts each distance twice.

It is interesting to note here that treatments by other authors such as Warren[12] include the use of an exponential convergence factor in K-space to make the problem soluble. It's assumed that these factors whether they are convergence factors or temperature factors are acting as integrating factors for the problem. The

treatment of the problem in any case will of necessity be inexact except in the case presented where it is assumed that all vibrational displacements in the lattice ensemble are equal. This assumption is of course invalid for polycrystalline experimental systems.

Rewriting the function G(R) in terms of both upper and lower limits of integration gives a function which represents the distribution function for a set of experimental data with a lower cutoff-limit of $K=M_1$ and an upper cutoff-limit of $K=M_2$.

$$4\pi R D_{\Delta}(R) = \frac{2}{\pi} \int_{M_1}^{M_2} F(K)\ \mathrm{Sin}(KR)\,dK \qquad (9)$$

where

$D_{\Delta}(R)$ = the G(R) function which would be obtained with a typical set of experimental data having respective vector termination values of M_1 and M_2.

F(K) = the interference function defined in equation 8.

Rearranging order of summation and integration gives

$$4\pi R D_{\Delta}(R) = \frac{2}{\pi} \sum_{\text{All J}} \frac{\bar{m}_J}{R_J} \int_{M_1}^{M_2} \mathrm{Sin}(KR_J)\mathrm{Sin}[KR]e^{-K^2\delta_J^2}dK \qquad (10)$$

The integral in equation 10 must be solved in the complex plane and the procedure is long. The solution may be found in the appendix section of the paper mentioned. The solution by Ergun[2] is given as:

$$4\pi R P_J(R) = \frac{2\bar{m}_J}{\pi R_J} \int_0^\infty \mathrm{Sin}(KR_J)\mathrm{Sin}(KR)e^{-K^2\delta_J^2}dK \qquad (11)$$

$$P_J(R) = \frac{\bar{m}_J(e^{-\alpha_J} - e^{-\beta_J})}{8\pi^{3/2}R_J\delta_J}$$

$$\alpha_J = (R_J - R)/2\delta_J$$

$$\beta_J = (R_J + R)/2\delta_J$$

$\mathrm{erf}(X)$ = Is the standard error function of X

$$\phi_J(m,\delta_J,R) = \frac{\bar{m}_J}{\sqrt{\pi R_J\delta_J}} \left[Z(M,\delta_J,\alpha_J) - Z(M,\delta_J,\beta_J)\right]$$

$$Z(a,b) = e^{-a^2}\frac{2}{\sqrt{\pi}}\int_0^b e^{(Y^2-b^2)}[\mathrm{Sin}(2aY)dY]$$

where

$$a = M\delta_J$$

$$b = (R \pm R_J)/2\delta_J$$

The function $P_J(R)$ is derived by changing the integration limits for equation 9, such that $M_1 = 0$ and $M_2 = \infty$.

Thus, G(R) which contains no termination error can be obtained by the summation of equation 11 over all interatomic distances. We can signify this function by an infinity (∞) subscript.

$$4\pi RD\ (R) = 4\pi R \sum_{All\ \ J} P_J(R) \qquad (12)$$

Equation 12 expresses a method for calculating G(R) from just knowledge of position, vibrational displacement, and the multiplicity of every interatomic distance. Or conversely experimental curves may be corrected to reflect data as though it were taken without termination. The key to utilizing these expressions comes from knowledge of m_J and δ_J both of which are difficult to obtain for complex experimental systems. For a theoretical system of the F.C.C. copper lattice as used in the computational models here, it would not be an unfair treatment to consider all of the δ_J equal. The parameter m_J could be computed from the array symmetry method described earlier; while δ_J^2 could be set equal to the expectation value of the mean-square displacement as arrived at by the summation of all the elastic waves in the system. Upon such considerations calculation of G(R) devoid of termination error becomes a trivial task. If this same function would need to be determined for experimental data it's absolutely necessary that all of the δ_J be set equal so that the error functions can factor out.

Figure 1 illustrates the variation of parameters M_2 and M_1. The displacement factor for this figure is $\delta_0 = 0$, which corresponds to a temperature of $T = 0^\circ$ Kelvin. Due to the uncertainty principle even at $T = 0^\circ K$ there is still a small displacement in the lattice, it's assumed to be zero. The effect of vector termination can be seen clearly in Curve A where $M_2 = 20\text{Å}^{-1}$. In this case the appearance

of termination satellites will be seen at $(\pm.4\ \text{Å}^{-1}) = (2\pi/K_{max})$ to the side of any major peak. These peaks are readily seen at r = 2.15Å; r = 2.95Å and at r = 4.05Å and r = 4.8Å. These satellites correspond to the major correlation distances r = 2.55Å and r = 4.42Å (see Ergun[2] and Warren[12]). Curve B shows the rapid washout of detail and peak broadening that occurs from vector termination due to the influence of the convoluted function $T(M_{2,x})$ described by Ergun.[3]

where

$$T(M_2,x) = \frac{M_2}{\pi}\left[\frac{\text{Sin}M_2(r-x)}{M_2(r-x)} - \frac{\text{Sin}M_2(r+x)}{m_2(r+x)}\right] \tag{13}$$

and

$$4\pi r D_\Delta(r) = \int_0^\infty 4\pi x\rho(x)\ [T(M_2,x)-T(M_1,x)]dx \tag{14}$$

where $D_\Delta(R)$ was previously defined in equations 9-11 and $\rho(x)$ is a delta like function which peaks at all interatomic distances. This is the function we would like to obtain by a deconvolution of the integral in equation 14. This sort of procedure is dependent on M_1 and M_2 and may not be able to be performed unless the analytical behavior of T(M,x) shows bounded support I,E (dies off rapidly with increasing x). There are many instances where T(M,x) may not be deconvoluted and other methods such as described previously must be used.

RADIAL DISTRIBUTION FUNCTION AND SMALL-ANGLE SCATTERING

The treatment of the exclusion of small-angle scattering (SAXS) on the RDF has been treated in depth by Cargill.[1] His treatment examined the SAXS associated with density fluctuations, and this makes his work very important for a material such as glassy carbon because of its high internal porosity. The data generated computationally in this paper contains SAXS associated with volume scattering and the effect upon the RDF is substantially different from the one noted by Cargill. The essential result revealed by Cargill is illustrated in equation 15. The result shows that the neglection of SAXS from the intensity kernel produces a G(R) which appears to correspond to a material of greater average atomic density than the material being studied. As a consequence of the slope of G(R) being disturbed near the first peak the coordination number of the first shell will be disturbed.

$$G_{exp}(R) = 4\pi R \left\{ \left(\rho(R)-\rho_o\right)\left[1 + \frac{\eta^2(\omega)\gamma(\omega,R)}{\rho_o^2}\right]\right\} \qquad (15)$$

where

$G_{exp}(R)$ = the Radial Distribution Function arrived at when SAXS is neglected from the interference function.

ω = a volume which is of the order of the atomic volume of the particle. This volume is associated with the Gaussian "Precision Function" used to approximate the contribution of SAXS due to density fluctuations.

$\eta^2(\omega)$ = the average of the square of the atomic density fluctuations.

$\gamma(\omega,R)$ = the density fluctuation correlation function.

The effect of neglecting SAXS yields a decrease in G(R) by the amount $(4\pi R\eta^2(\omega)\gamma(\omega,R)/\rho_0)$ which introduces an error of $(4\pi R\eta^2(\omega)/\rho_0)$ at small values of R where the density fluctuation correlation function is near unity.

Since the particle sizes in this problem are so small the unobservable peaks are clearly visible (see Figure 7a). These unobservable peaks are usually never seen in experimental situations. They are, however, responsible for contributing the amount $4\pi R\rho_0$ in the G(R) curve negatively and can be interpreted as the changing of ρ_0 to a smaller value for all G(R) values computed in this paper which include volume scattering in the intensity kernel. See Figure 3 which shows the contribution to G(R) from volume scattering.

Figures 2 and 4 shows the intensity and G(R) functions for a cube-shaped particle of size N = 4 on an edge. Where Figure 2 contains SAXS and Figure 4 does not. The overlay of Figures 2 and 4 is shown as Figure 5.

The results for Figures 2, 4 are shown in Table 1. The effect of low-angle cut-off ($M_1 = 2.3\text{Å}^{-1}$) is responsible for the slope seen in Figure 4 as compared to Figure 2 which shows a zero slope in the small-R region. The calculations of SAXS for any M_1 cutoff is calculated by smoothing the interference function in the region

$K = 0\text{Å}^{-1}$ to $K = M_1\text{Å}^{-1}$. The Porod region is located and the constant relating its behavior is determined. This constant is then used to subtract the analytic expression for volume scattering (see Warren[12]).

$$\frac{I.E.U(K)}{4N^3} \text{ volume scattering} = \frac{4\pi R^3 \rho_o}{3} f^2_{(K)} \phi^2(KR) \qquad (18)$$

where:

$4N^3$ = the number of atoms in the ensemble

ρ_o = macroscopic density

$f(K)$ = atomic scattering factor

$$\phi^2(KR) = \frac{9}{(KR)^4}\left(\frac{\text{Sin}KR}{KR} - \text{Cos}KR\right)^2$$

$$K = \frac{4\pi \text{Sin}\theta}{\lambda}$$

Rewriting eq. 18 gives a Porod approximation

$$I.E.U(K)_{\text{volume scattering}} = \frac{Cf^2(K)\langle\phi^2(KR)\rangle}{} = \frac{C'f^2(K)}{K^4} \qquad (19)$$

where

$\langle\phi^2 KR)\rangle = \frac{9}{2(KR)^4}$ which is the expectation value of the interference function for SAXS for spherical particles.

Since the particle is a cube its "gamma" function ($\gamma_o(R)$) will be different and this will mean a different scattering function is actually applicable (see Guinier, Fournet).[16] Thus, the analysis is not exact.

The coordination analysis shows that the contribution of volume scattering (SAXS) to the RDF profile must be corrected for by altering

ρ_0 (see Table 1). The new ρ_0 may be calculated from the negative shift observed. This is possible since peak-positions and area are conserved. Table 1 does not account for the shift observed and thus different coordination numbers are reported. The coordination numbers reported with (SAXS) removed are correct to within experimental error. As mentioned, the influence of particle size and the intensity of SAXS at angular values outside of the direct beam are directly observed. This has applicability to a material such as glassy-carbon since its pore sizes are small, on the order of $R_g = (10 - 20)\text{Å}$ (see (Hoyt).[17] R_g is the electronic radius of gyration and for a spherical particle would just be its radius.

PARTICLE SIZE AND INTERPARTICLE INTERFERENCE AND INFLUENCE UPON RDF

The effect of particle-size broadening on the profile in K-space has been well documented. The classical papers are those by Scherrer and (Stokes and Wilson).[9] The derivation of their equations may be found in practically any college-level textbook dealing with diffraction. In a material such as glassy carbon where the presence of faulting and strain are present along with particle size, the use of the above methods have very limited value.

This paper does not apply strictly to glassy carbon, however it will show how the evolution of particle size may be traced using the RDF. To make the method applicable for glassy carbon would require a strain analysis such as the Warren-Averbach method (see Wagner[18]). The analysis for faulting might then be completed in R-space using the method of Ergun[3] where the Cosine transform of (001) reflections are curve-fitted to an exponential form.

For a material such as glassy carbon we need to consider the effects of layer size, strain, and faulting. Ergun[3] has chosen to write the interference function for glassy carbon as:

$$J(h) = \sum_{\text{all } l_q} n(l_q)g(l_q)f(h,l_q)\frac{\text{Sin}(hl_q)}{hl_q} \qquad (20)$$

$$h = \frac{4\pi \text{Sin}\theta}{\lambda}$$

$n(l_q)$ = the total number of interatomic vectors of length l_q

$g(l_q) = (e^{-\alpha l_q})$ which modifies $n(l_q)$ to account for interlayer stacking defects and finite lattice size. Where α is a defect correlation distance given as: $\alpha = (2/d)$. d = mean distance between defects between layers. $f(h,l_q)$ = a factor used to account for temperature vibration and strain in the lattice.

The similarity of equation 20 and equation 8 are immediately visible except for the omission of $g(l_q)$ and the average of $n(l_q)$ from equation 8. The similarity of equation 20 and equation 1 (the Debye sum) can be immediately recognized also. The result arrived at by computation in this paper only expresses the effect of $n(l_q)$ upon the RDF and this function is known and expressible for any lattice in set notation (see Ergun[19]). Since $n(l_q)$ is independent of the scattering vector, the function G(R) is only product dependent upon $n(l_q)$. Since $n(l_q)$ is a function of particle size, G(R) can be used as a measure of particle size when temperature and strain effects are not present in the interference function as expressed by the function $f(h,l_q)$. The function $g(l_q)$ which was used to account for a defective lattice will necessarily be included in $n(l_q)$ since its also scattering vector independent. Ergun[3] has outlined a method for seperating $n(l_q)$ and $g(l_q)$ so as to arrive at d, the mean-defect-free interlayer distance.

The relationship of SAXS to particle size through "radius of gyration" calculation are explored extensively in such texts as (Guinier and Fournet)[16] and the relationship of the correlation function to specific surface area are shown by Debye.[14] The problem

being solved in this study involves an ideal gas composed of copper particles of a single size. We can write the intensity function in terms of a volume scattering term and a perturbation volume term from (Guiner and Fournet)[16]

$$I.E.U(K) = \bar{N}I_1(K) + I_e(K)\bar{N}F^2(K)\left[1 - \frac{V_2}{V_1}\right] \qquad (21)$$

where

$I_1(K)$ = the scattering due to the volume of the particle (see equation 21).

$\bar{N}$ = the average number of particles in the scattering volume.

$F^2(K)$ = the structure factor of the material being studied.

V_1 = the average total volume available per particle.

$V_2 = \int_0^\infty 4\pi R[1 - p(R)] \operatorname{Sin} \frac{(KR)}{K} dR$ referred to as the perturbation volume.

$I_e(K)$ = the scattering of a single electron for non-polarized radiation.

$P_{(R)}$ = probability of finding a pair of atoms seperated by a distance R, when the atoms are in different particles.

The term $I_1(K)$ expresses SAXS due to volume scattering and it is this term which gives rise to scattering in the Guinier and Porod regions. The result from equation 21 is the same result as $I_1(K)$ if $I_1(K)$ is evaluated using the Fraunhofer approximation with a flat-faced diffractometer sample. Rewriting equation 21 yields

$$I.E.U(K) = NI_e(K)\left[I_1(K) - \frac{V_2}{V_1}F^2(K)\right]_{\text{SAXS TERM}} \qquad (21A)$$

$$+ I_e(K)N\,F^2(K)_{(\text{WAXD-Intensity TERM})}$$

Exploring the behavior of the ratio (V_2/V_1) for different systems gives much insight as to how interparticle effects control the interference function and thus the RDF. For the system computed in this paper we can easily show that there is no prefferred orientation of particles and as such the quotient $(V_2/V_1) = 0$. The RDF obtained by transforming equation 21 with this condition will create a G(R) function with a zero-slope in the small R region as illustrated in Figure 2 where the slope at small-R is flat.

In any system such as glassy carbon the value of (V_2/V_1) will be non-zero due to the large internal porosity of the material and the density fluctuations between lathes. When interparticle effects become non-negligible it's necessary to rewrite the intensity function either in terms of Thermodynamic variables or in terms of potential energy expressions. The effect of interparticle interference will always be to decrease the SAXS K^{-4} law so that the corresponding G(R) function must possess a negative slope at small-R.

Table 2 shows the Scherrer analysis for the (002) reflection. The Scherrer equation gives an excellent approximation of true particle size. Table 3 shows both peak height and width for G(R) for the first three coordination shells for the particle sizes N = 2; N = 9 for all

three particle shapes. The evolution of peak width in K-space is expressed by the Scherrer equation (eq. 22). While the relation between the correlation function and interference function in terms of particle size is expressed by a "free electron" volume described by Debye[4] in equations 23, 24 and 25. The evolution of the RDF with particle size is shown in Figures 7-9, and table 3.

$$\beta(2\theta) = \frac{\lambda}{L \cos\theta_\beta} \qquad \text{Scherrer Equation} \qquad (22)$$

where

$\beta(2\theta)$ = the full width at half-maximum intensity measured in radians for a reflection associated with the crystallite dimension L.

L = the crystallite dimension in angstroms associated with the plane reflection being examined.

θ_β = the Bragg-angle of the plane reflection being examined.

The Scherrer equation is valid for reflections having no broadening due to instrumental effects, crystal strain or fault broadening. Thus, all figures presented can be analyzed using the Scherrer equation.

Debye has expressed a "free electron" number (η^*) as the scattering due to the total number of electrons π in the scattering volume V.

$$\eta^* = VAv \langle(\delta\eta)^2\rangle^2 \int_0^\infty \frac{C(R)\mathrm{Sin}(KR)d\tau}{KR} \qquad (23)$$

where

V = volume illuminated by the primary beam.

$Av<(\delta\eta)^2>$ = the expectation value of the square of free electron density fluctuation per cubic centimeter, evaluated for small atomic seperation distances.

$d\tau$ = a volume element defined by R and θ.

The integral in equation 23 represents an effective scattering power contained in the illuminated volume V as observed at K. This knowledge then leads directly to a relation between the correlation function C(R) and the volume expressed by its Fourier Transform. Debye expresses this volume function as (K) where:

$$(K) = \int_0^\infty C(R) \frac{Sin(KR)}{KR} d\tau \qquad (24)$$

C(R) = the correlation function for the material as defined by Debye.

Equation 24 is an expression of the electron volume participating in scattering and can be associated with particle size when the volume element $d\tau$ is evaluated for a case such as spheres at K = 0. The relation between this volume and this scattered intensity is given by equation 25.

$$\frac{I(K)}{I_o} = \left(\frac{e^2}{mc^2}\right)^2 \frac{(1+\cos^2\theta)}{2r^2} \eta^*(K) \qquad (25)$$

where

$\left(\frac{e^2}{mc^2}\right)^2$ = the scattering cross section of a free electron.

$\frac{(1+\cos^2\theta)}{2}$ = polarization factor for an unpolarized primary beam.

r = the distance from the sample to the point of observation.

Equation 25 is significant in showing the proportionality between intensity and "free electron volume". Equation 25 may be rearranged to yield a result given by Guinier[16] shown in equation 29.

$$\overline{F^2}(K) = F^2(0) \int_0^\infty \gamma_0(R) \frac{\sin(KR)}{KR} \, d\tau \tag{26}$$

where

$d\tau = 4\pi R^2 dR$

$\gamma_0(R)$ = a correlation or "characteristic function" of the particle. Its definition is that it represents the probability that an arbitrary point at a distance R in a random direction from a fixed point in the particle will itself be in the particle.

The equivalence of equations 25 and 26 can be shown by equating $\gamma_0(R)F^2(K)$ and $VA\nu\langle(\delta\eta)^2\rangle C(R)$. This can be easily shown since Debye defines $\eta^*(K)$ in the Porod region identically to $F^2(K)$.

$$\eta^*(K) = \overline{F^2}(K) = (2\pi\rho^2 S/K^4) \tag{27}$$

when $(KR_1 > 2\pi)$

where

R_1 = radius of particle undergoing diffraction

ρ^2 = square of electron density of particle.

Further it can be shown that the integral of $\gamma_o(R)$ over all R is one half of the average particle size. Table 3 exhibits the growth in amplitude of the first peak in G(R) for three different shape particles. All peak widths remained constant within measurement limits. The peak heights showed a limiting behavior as particle size was increased. See figures 7-9 and Table 3. Where figures 7-9 represent the growth in coordination number vs. particle size and Table 3 shows the growth of G(R).

PARTICLE SHAPE AND ITS EFFECT UPON THE RDF

Particle shape influences the scattering curve at small angles and as such it will be shown that its effect on G(R) is negligible for large particle sizes. Scattering curves for various shaped particles have been calculated by such people as Kratky and Porod and Rayleigh. These curves can be shown to have similar characteristics in that they will all tend to zero, oscillating about a K^{-4} curve as long as $K >> (1/\epsilon)$; where ϵ represents the small dimension for anisotropic shapes such as discs or cylinders. The Zernicke-Prins equation and other similar derivations all involve the neglection of scattering at small angles where the shape of the volume exerts its influence. In typical experimental data this intensity will be covered by the primary beam. The actual G(R) curve which will be derived from experimental intensity will be a difference function as shown by Riley.[5]

$$\left[G(R) - \phi(R)\right] = \frac{2R}{\pi} \int_0^\infty Ki(K)Sin(KR)dK \qquad (28)$$

where:

M_1 = the low-angle cut-off for the experiment

$i(K)$ = the experimentally observed interference function.

$\phi(R)$ = the "shape function" defined as the Fourier transform of the unobserved low-angle scattering for an amorphous particle of uniform electron density.

The seperation of $\phi(R)$ is impossible, since its analytical form is not known for systems of particles found in non-dilute experimental

situations. In the case of a very dilute system or theoretical system, as in the Debye sum, $\phi(R)$ is equivalent to $\gamma_o(R)$ the characteristic function of the particle. The information of a particle size will be found at the largest R-values observable in the RDF. In reciprocal space this information should be in the SAXS region, and this implies that the correction of SAXS should have an effect upon the RDF peaks at large R. However, examination of the "characteristic function" shows that it takes on its largest value at R = 0 and falls to zero at distances approaching and or equal to the particle size. For example, a sphere of radius R_s will have a $\gamma_o(R)$ function defined by equation 29. From inspection one can determine the function is zero at $R = 2R_s$.

$$\gamma_o^{sphere}(R) = 1 - \frac{3R}{4R_s} + \frac{1}{16}\left(\frac{R}{R_s}\right)^3 \qquad (29)$$

Equation 29 illustrates how the function $\gamma_o(R)$ would be useful in determining characteristic particle size. However, the equation really contains no information on the shape of the particle and it's possible that two different shaped particles could have very similar $\gamma_o(R)$ since $\gamma_o(R)$ is dependent upon the surface to volume ratio of the particle. The illustration of $\gamma_o(R)$ approaching zero can be found in Figure 5 where the RDF functions approach identical values at R = 14.50Å. This is to be expected from a particle whose characteristic dimension is of this order.

The effect of particle shape will be to change the function $\gamma_o(R)$; which would be equivalent to changing $n_J(R_J)$ in equation 8. The change in this function may be monitored directly by comparing peak-height ratios in G(R).

The absence of a specific pattern can sometimes be related to its shape. For example, an F.C.C. structure in the shape of a rod cannot contain distances expressed as the square root of an integer which has as its square root a non-integer number. I.E.

$$R_{IJ}^{rod} \neq \sqrt{2}a,\ \sqrt{3}a,\ \sqrt{5}a,\sqrt{6}a,\ \sqrt{7}a,\ \sqrt{8}a,\ \sqrt{10}a \quad \text{etc.}$$

These distances are allowed for a plate or cube shape and other methods need to be used to distinguish these shapes. One method which can be determined qualitatively but is not offered here as a quanitative method is to ratio the peaks found at a, and 2a. It should be noted that these ratios will be a function of particle size and will not converge until that size becomes much larger than 2a.

A preferred method of determining shape is in examining the intensity curve in reciprocal space. The Scherrer analysis of Figure 6a reveals the particle has well developed structure of (111) type planes. In comparison plate and rod shapes show poor development of these planes (see 6b and 6c). This information in conjunction with Scherrer analysis allows speculation as to the shape of a particle. In a formal sense the sensitivity of the two methods should be identical since both methods are manifestations of the same reality. In practice however differences in structure tend to be more localized

in curves in reciprocal space as compared to the effects in real-space. Both curves have their advantages in certain situtations, but in conjunction with each other they form a powerful tool when interpreting experimental data against scattering models constructed computationally.

DISCUSSION AND CONCLUSIONS

The results obtained by Fourier inversion of Small-Angle data (SAXS) show that this portion of the intensity is associated with the effective density of the material and particle size. The importance of SAXS subtraction when dealing with only volume scattering is found in the Zernicke Prins equation and discussed by Cargill,[1] Franklin,[24] Diamond,[23] and Warren.[12] The removal of SAXS and application of gaussian analysis provided answers for coordination numbers within experimental error. See Table 1, which shows the results of coordination numbers obtained with and without Saxs data. Peak-position was always conserved regardless of Saxs. Evidence is found in figure 5 which shows an overlay of RDF patterns which include and exclude Saxs in their intensity kernel. The figure clearly shows the superposition of peaks. Peak area was also found to be conserved, however the ρ_o is shifted to some unknown value when Saxs is included in the transform. This area conservation is best demonstrated by figure 5, which shows both patterns as identical but displaced by the amount shown in figure 3.

The results obtained from the diffraction data at higher angles (WAXD) is completely accurate to within experimental error as demonstrated by figures 6a, b, and c which show convincing WAXD patterns accurate to within $\pm.05\text{Å}^{-1}$ for a cube, plate and rod structure. Also the Fourier transforms of this data which illustrate the interatomic distances were accurate to within ±.05Å. From these results and the coordination number results obtained in figure 7 it

appears as though the model's discontinuity has not interferred with the data obtained in real or reciprocal space. The primary results of this study are reflected in figures 7, 8 and 9. Close examination of these figures demonstrate conclusively that the first coordination shell stops evolving with an effective particle size of 30-40Å. All of the shapes studied confirm this result so shape appears to play no role.

The results for the second and third coordination shells must be obtained from figures 8 and 9, since the particle size in the three dimensional model is not large enough for the second or third shell to have converged. There appears to be no easy way to confirm these results since they are based on the one and two dimensional models of the plate and rod. The result for the second shell appears to be that it has converged at particle sizes on the order of 90Å as shown in figure 8. Figures 8 and 9 indicate that the third shell is fully evolved at an effective particle size of ~130Å. Since the effective particle size in figure 9 is increasing so rapidly the interpolation is best taken from figure 8. Since figures 8 and 9 represent data from one and two dimensional models respectively, the results may not apply to experimental situations and care should be used in transferring these results to experimental situations.

Table 1. Effect of SAXS

Shape = Cube						
R	G(R)	$(G(R))_{corr}$	Coordination No.	Coordination No. Corrected	Actual Coordination No.	N
2.55	25.70	23.21	10.96	10.00	12	4
4.45	23.82	21.64	19.22	17.75		4
5.75	18.22	18.02	21.16	20.99		4
2.55	29.92	26.96	12.58	11.40	12	9
4.45	32.25	28.58	24.89	22.42		9
5.75	28.46	23.52	30.07	25.77		9

Table 2.

	Na	L^{*}_{002}		ΔK_{002}
N	Å	Å	Shape	$Å^{-1}$
4	14.45	14.21	Cube	.442
7	25.30	25.50	Cube	.246
9	32.53	33.42	Cube	.188

*$L_{002} = 2\pi/\Delta K_{002}$

Table 3

N	Shape	G(R) atoms/Å^2	ΔG(R) Width at half max ±.02Å	Coordination No.	R Å
2	Cube	19.40	.17	8.53	2.55
3	Cube	23.44	.17	10.09	2.55
4	Cube	25.70	.17	10.96	2.55
5	Cube	27.16	.17	11.52	2.55
6	Cube	28.17	.17	11.91	2.55
7	Cube	28.91	.17	12.19	2.55
8	Cube	29.48	.17	12.42	2.55
9	Cube	29.92	.17	12.58	2.55
2	Plate	17.26	.17	7.70	2.55
3	Plate	19.39	.17	8.52	2.55
4	Plate	20.37	.17	8.90	2.55
5	Plate	20.93	.17	9.12	2.55
6	Plate	21.29	.17	9.26	2.55
7	Plate	21.50	.17	9.34	2.55
1	Rod	7.36	.17	3.88	2.55
2	Rod	11.74	.17	5.57	2.55
3	Rod	12.18	.17	5.74	2.55
4	Rod	12.33	.17	5.80	2.55
5	Rod	12.40	.17	5.83	2.55
2	Cube	6.48	.17	10.95	5.75
3	Cube	13.97	.17	17.47	5.75
4	Cube	18.22	.17	21.16	5.75
5	Cube	21.24	.17	23.79	5.75
6	Cube	23.39	.17	25.66	5.75
7	Cube	26.74	.17	28.58	5.75
8	Cube	27.71	.17	29.42	5.75
9	Cube	28.46	.17	30.07	5.75
2	Plate	5.95	.17	10.49	5.75
3	Plate	9.79	.17	13.83	5.75
4	Plate	11.65	.17	15.45	5.75
5	Plate	12.68	.17	16.34	5.75
6	Plate	13.32	.17	16.90	5.75
7	Plate	13.75	.17	17.28	5.75

Table 3 cont

N	Shape	G(R) peak atoms/Å2	ΔG(R) Width at half max	Coordination No.	R Å
1	Rod	-0	.17	0	5.75
2	Rod	4.17	.17	8.94	5.75
3	Rod	4.83	.17	9.52	5.75
4	Rod	4.99	.17	9.65	5.75
5	Rod	5.11	.17	9.76	5.75
2	Cube	11.24	.17	10.75	4.45
3	Cube	18.95	.17	15.94	4.45
4	Cube	23.82	.17	19.22	4.45
5	Cube	26.88	.17	21.28	4.45
6	Cube	28.82	.17	22.58	4.45
7	Cube	30.26	.17	23.55	4.45
8	Cube	31.37	.17	24.30	4.45
9	Cube	32.25	.17	24.89	4.45
2	Plate	6.58	.17	7.61	4.45
3	Plate	9.23	.17	9.39	4.45
4	Plate	10.52	.17	10.26	4.45
5	Plate	11.29	.17	10.78	4.45
6	Plate	11.74	.17	11.09	4.45
7	Plate	12.01	.17	11.27	4.45
1	Rod	0	.17	0	4.45
2	Rod	2.72	.17	5.02	4.45
3	Rod	3.01	.17	5.21	4.45
4	Rod	3.16	.17	5.31	4.45
5	Rod	3.25	.17	5.37	4.45

REFERENCES

1. G. S. Cargill III, "Influence of Neglected Small-Angle Scattering in Radial Distribution Function Analysis". J. Appl. Cryst. 4 (1971) 277.

2. J. R. Townsend and S. Ergun, "Analysis of Termination Effects on Atomic Radial Density Curves." Carbon 6 (1968) 19.

3. S. Ergun and R. Schehl, Analysis of the Structure of a Glassy Carbon Using the Fourier Transform Technique". Carbon 11 (1973) 127.

4. P. Debye, "Scattering of Radiation by Non-Crystalline Media". Conference on Non-Crystalline Solids, Sept. 3-5, 1958, John Wiley and sons (1960).

5. D. P. Riley, "Spherically Symmetric Fourier Transforms and Medium Range Radial Distribution Functions in the X-Ray Determination of Complex Molecular Structures" Conference on Non-Crystalline Solids, Sept. 3-5, 1958, John Wiley and sons (1960).

6. H. Fichtner-Schmittler, K. Fichtner, Computer Generation of Composite X-ray Powder Patterns. Kristall UndTechnik, 13 (Suppl. 8) (1978), 1009.

7. Klug, H. P., Alexander, L. E., X-Ray Diffraction Procedures for Polycrystalline and Amorphous Materials 2D, Ed., New York, Wiley (1974).

8. R. L. Cassola, "Floating Point Algorithm Design". Computer Design, June (1982), 107.

9. A. R. Stokes and A. J. C. Wilson, Proc. Camb. Phil. Soc. 38 (1942) 313.

10. R. Kaplow, "Interatomic Potentials; Aspects Which are Visible in Experimental Radial Pair Distributions". In: Interatomic Potentials and Simulations of Lattice Defects, Gehlen, Beeler and Jaffee, Plenum Press (1972).

11. J. E. Enderby and W. S. Howells, "Experimental Techniques Used to Obtain Potentials". IBID (see above).

12. B. E. Warren, X-Ray Diffraction, Addision S. Wesley, 1969.

13. G. Stell, Physica 29 (1963) 517.

14. R. Kaplow, S. L. Strong, and B. L. Averbach, "Radial Density Functions for Liquid Mercury and Lead". Physical Review 138 (Suppl. 5a) (1965) A1336.

15. Curtis Gerald, "Applied Numerical Analysis" 2nd Edition, Addison-Wesley (1980), pg. 214-215.

16. A. Guinier, G. Fournet, "Small Angle Scattering of X-Rays", Wiley and Sons (1955), pg. 13-24.

17. J. Hoyt. "A Study of Pore Growth in Glassy Carbon using Small-Angle-Scattering", M.S. Thesis, Lawrence Berkeley Laboratory, 1983.

18. C. N. J. Wagner and E. N. Aqua, "Analysis of the Broadening of Powder Pattern Peaks from Cold-Worked Face-Centered and Body-Centered Cubic Metals," In: Advances in X-Ray Analysis 7, Mueller, Mallett, and Fay. Plenum Press, New York.

19. Ergun, S., Phys. Rev. B1, 3371 (1970).

20. James, R. W., The Optical Principles of the Diffraction of X-rays, (1948), Bell London.

21. Wignall, G. D., Pings, C. J.. "Structure of Vitreous Carbon from Wide Angle and Low Angle X-Ray Diffraction." Carbon 12 (1974) 1.

22. R. W. Lindberg, M.S. Thesis, Stanford University (1969).

23. Diamond, R. "X-Ray Diffraction Data for Large Aromatic Molecules". Acta Crystallographica 10 (1957) 359.

24. Franklin, R. E., "The Interpretation of Diffuse X-Ray Diagrams of Carbon", Acta Crystallographica 3 (1950) 101.

25. Suzuki, K. Science Reports of Tohuku University (1978).

FIGURE CAPTIONS

Fig. 1. Shows the effect of termination error upon resolution of peaks in the RDF. Both curves are for cubes of side-length (N = 3). Curve A shows termination at K = 20Å^{-1}, and Curve B shows termination at K = 5Å^{-1}.

Fig. 2. Shows the RDF for a cube of side-length (N = 4). This distribution was produced from data taken from K = .05Å^{-1} to K = 20Å^{-1}. The flat zero slope in the small R region is indicative of the presence of volume scattering in the transformed intensity function.

Fig. 3. Shows a Saxs transform of the intensity region K = .05Å^{-1} to K = 2.3Å^{-1}. The contribution of this curve to G(R) should be $4\pi R\rho_0$ out to (Na/2). The intensity data is extracted from figure 2 and represents Saxs for a cube of side-length (N = 4).

Fig. 4. This figure shows the result of transforming intensity data without Saxs (volume scattering). The intensity data used in this transform is the same as figure 2 except the limits extend from K = 2.3Å^{-1} to K = 20Å^{-1}.

Fig. 5. This figure demonstrates the effect of the $\gamma_0(R)$ function by showing the overlay of figures 2 and 4. Note the convergence of the two curves at R = 14.5Å. Note also the exact overlay of peak position, demonstrating Saxs has no effect on RDF positions.

Fig. 6a, b,c These figures show overlays of WAXD for the shapes and sizes indicated on the figures. These figures also illustrate the evolution of the specific planes associated with each shape and how particle size effects sharpness in reciprocal space.

Fig. 7. The coordination number for cube shaped particles for the first three coordination shells is plotted versus the effective particle size. Since the data transformed contains Saxs, the asymptote of the first coordination shell curve rises above the theoretical line shown.

Fig. 8. The coordination number for plate shaped particles for the first three shells is plotted versus the effective particle size which is N^2a for plates. Note that the asymptote of the first shell begins at the same value as that for cubes.

Fig. 9. The coordination number for rod shaped particles for the first three shells is plotted versus the effective particle size which is N^3a for rods. Note that the asymptote of the first shell begins at the same value as that for cubes and plates.

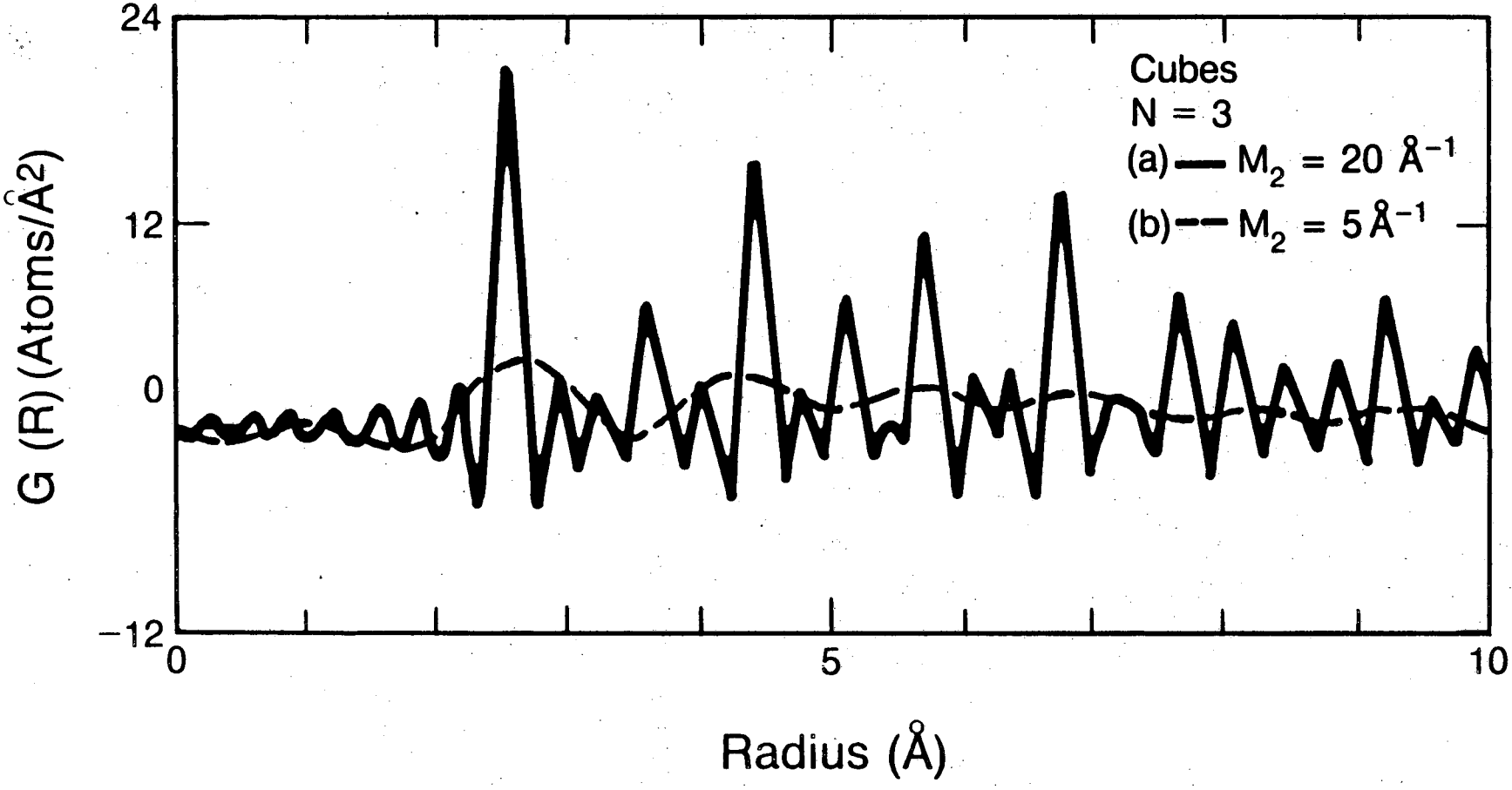

50

Figure 1

XBL 845-9362

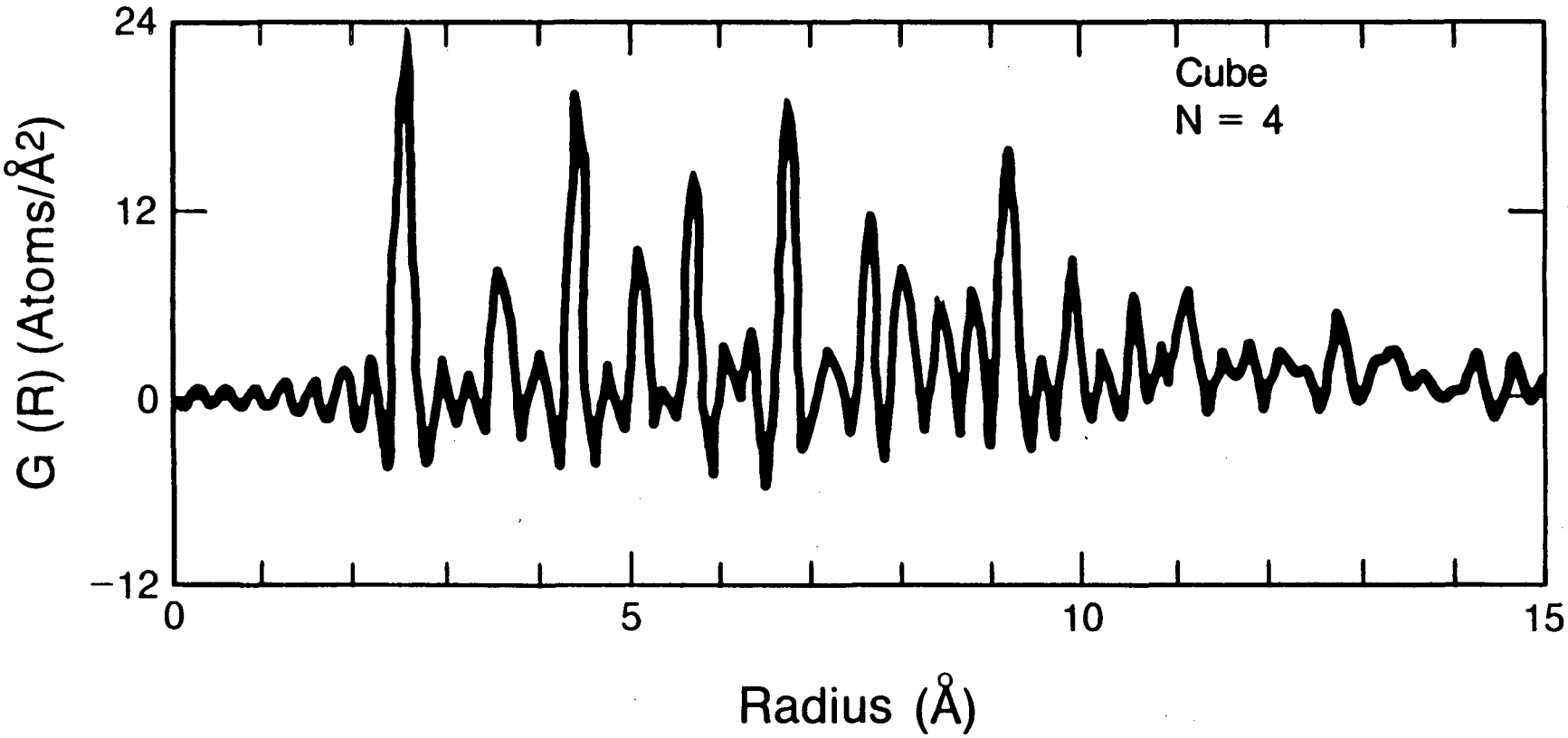

Figure 2

XBL 845-9361

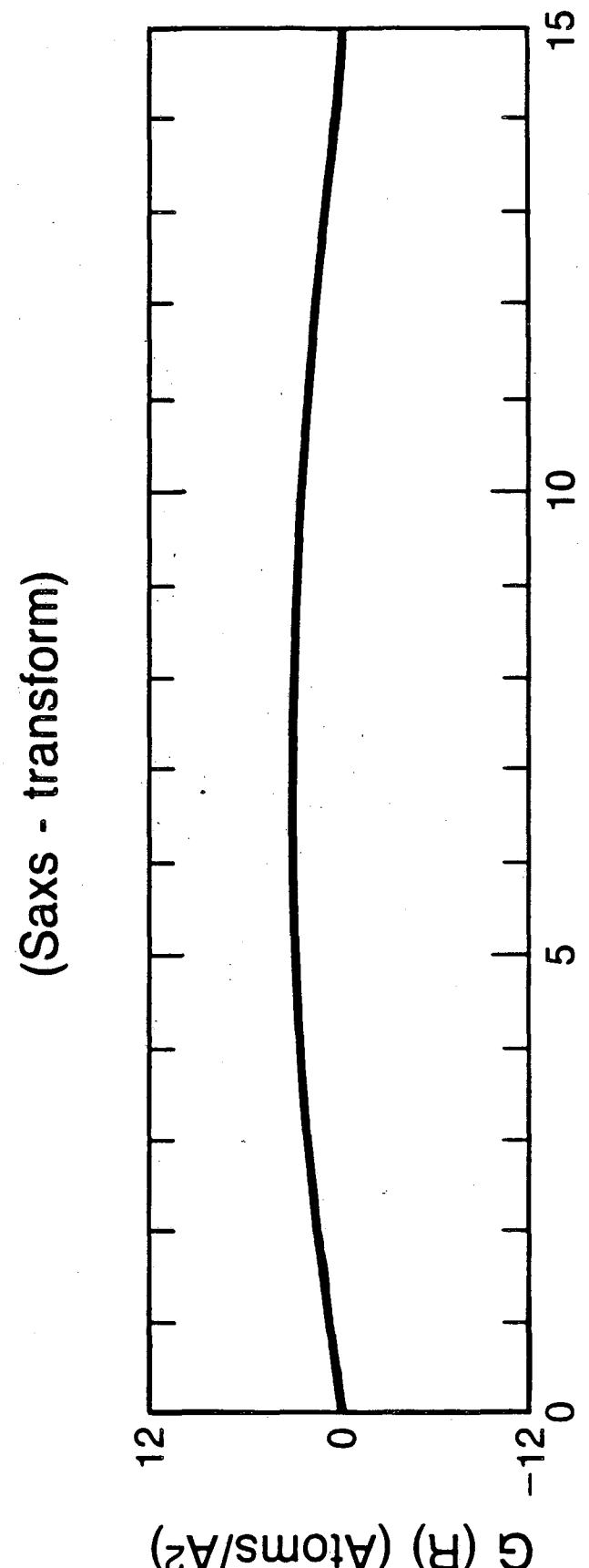

XBL 845-9363

Figure 3

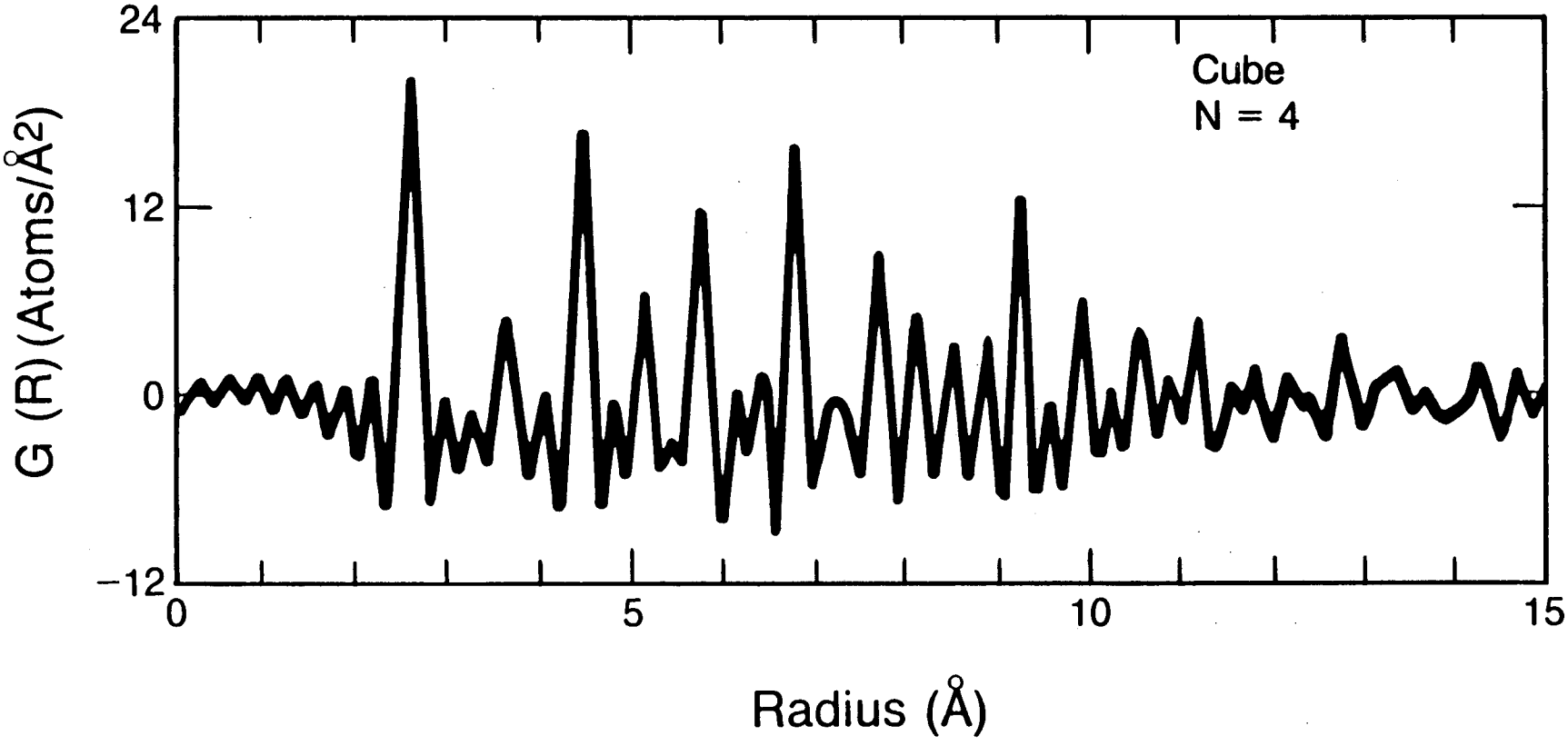

Figure 4

XBL 845-9360

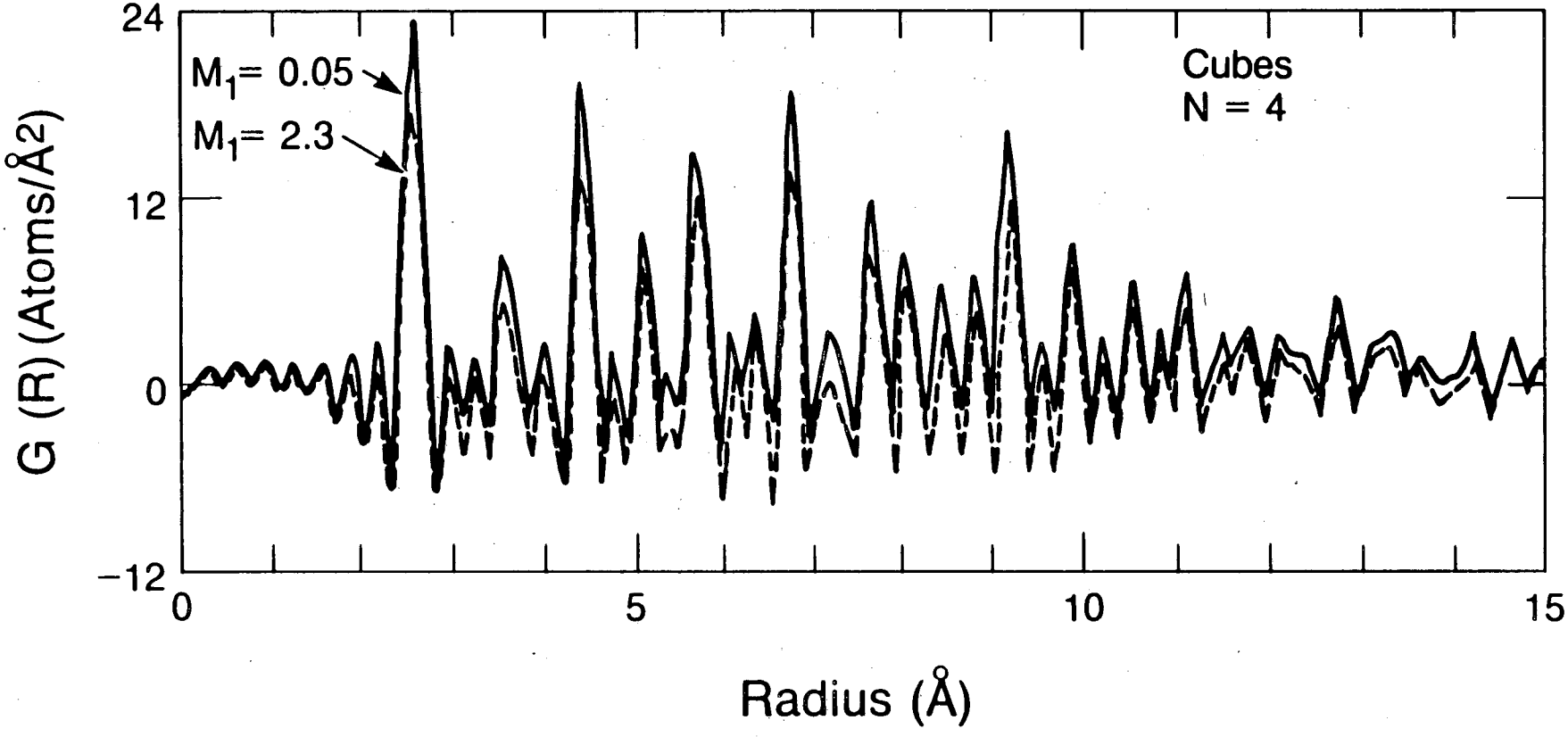

Figure 5

XBL 845-9359

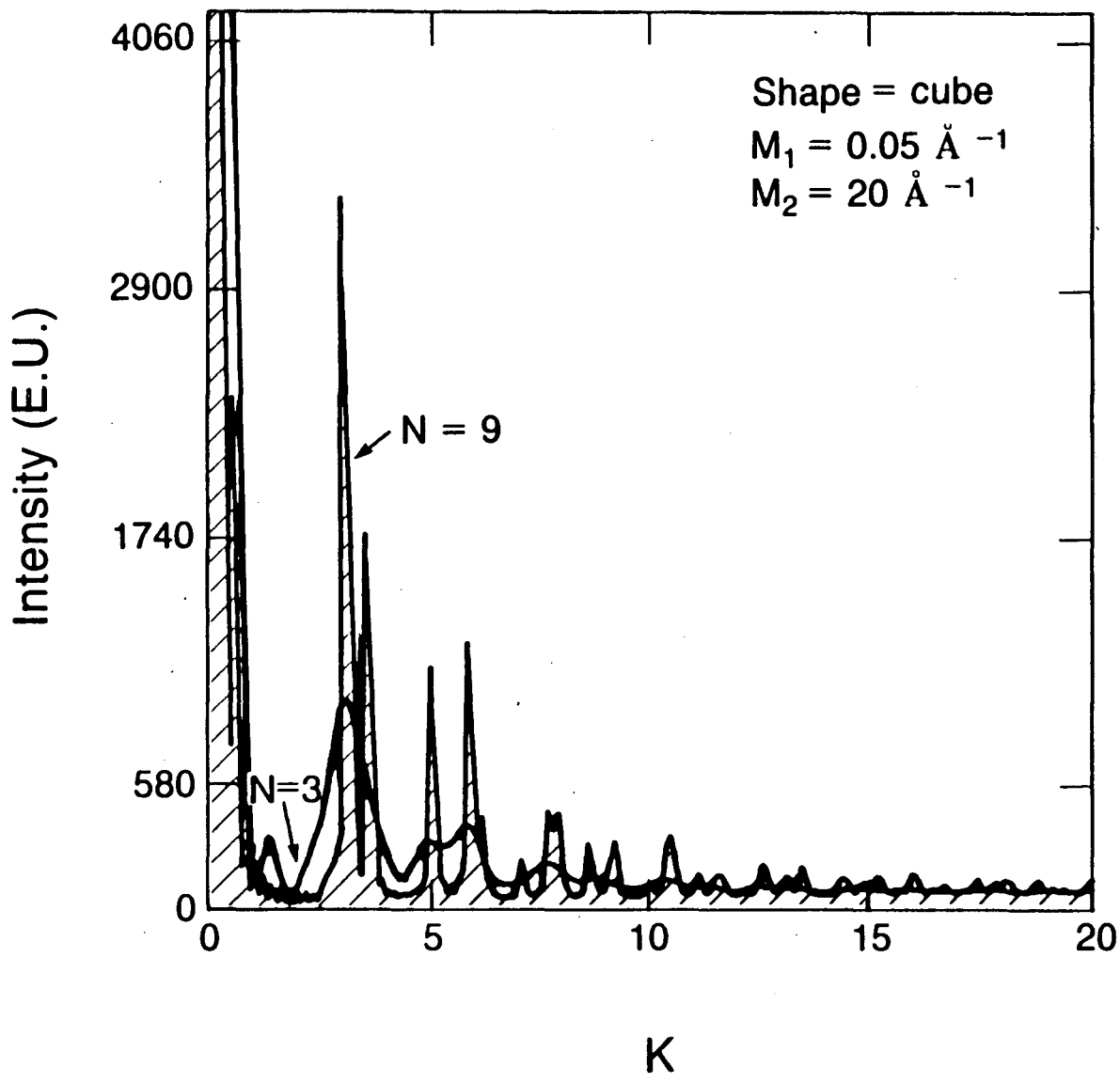

Figure 6a

XBL 844-10419

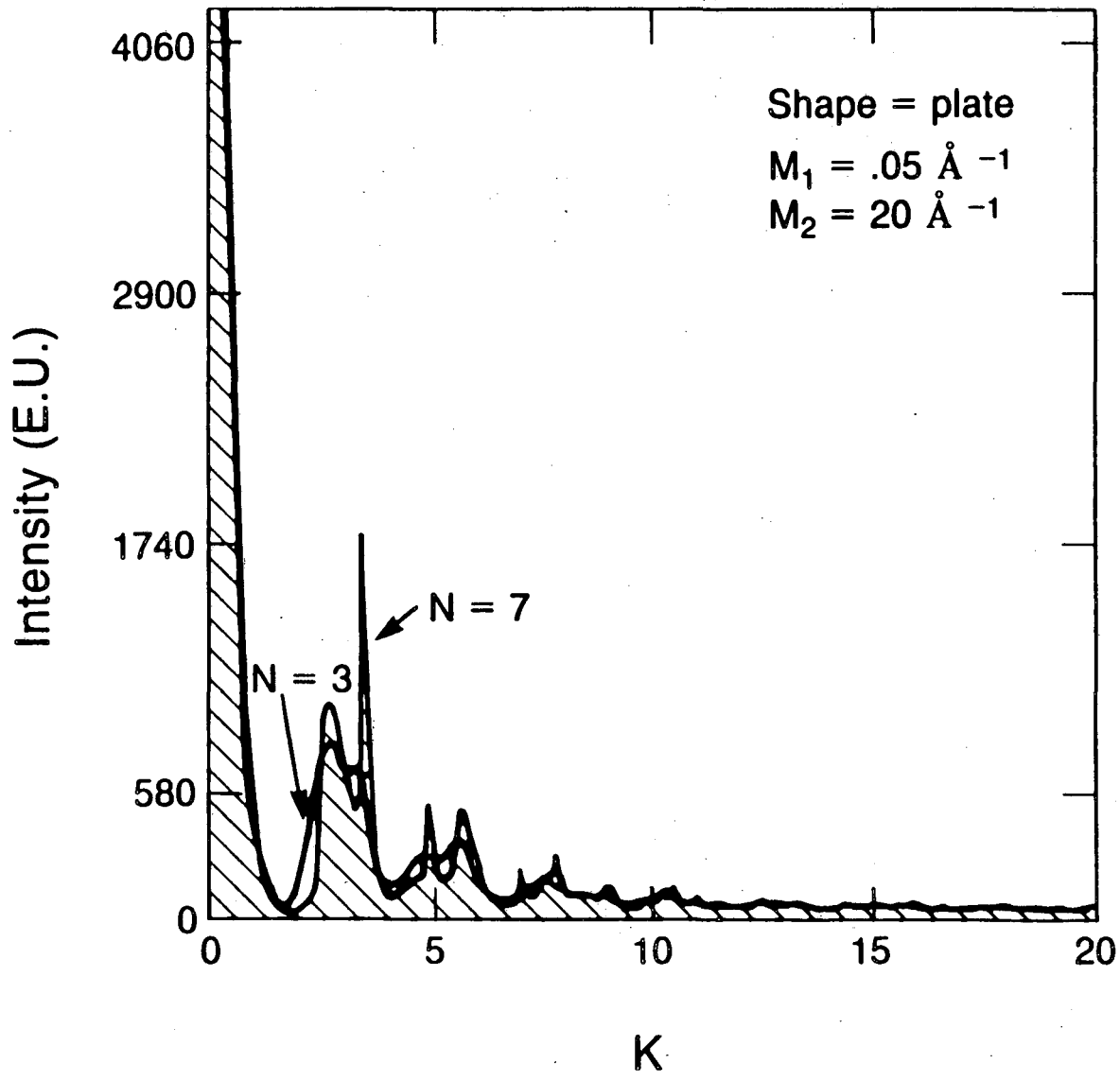

Figure 6b

XBL 844-10423

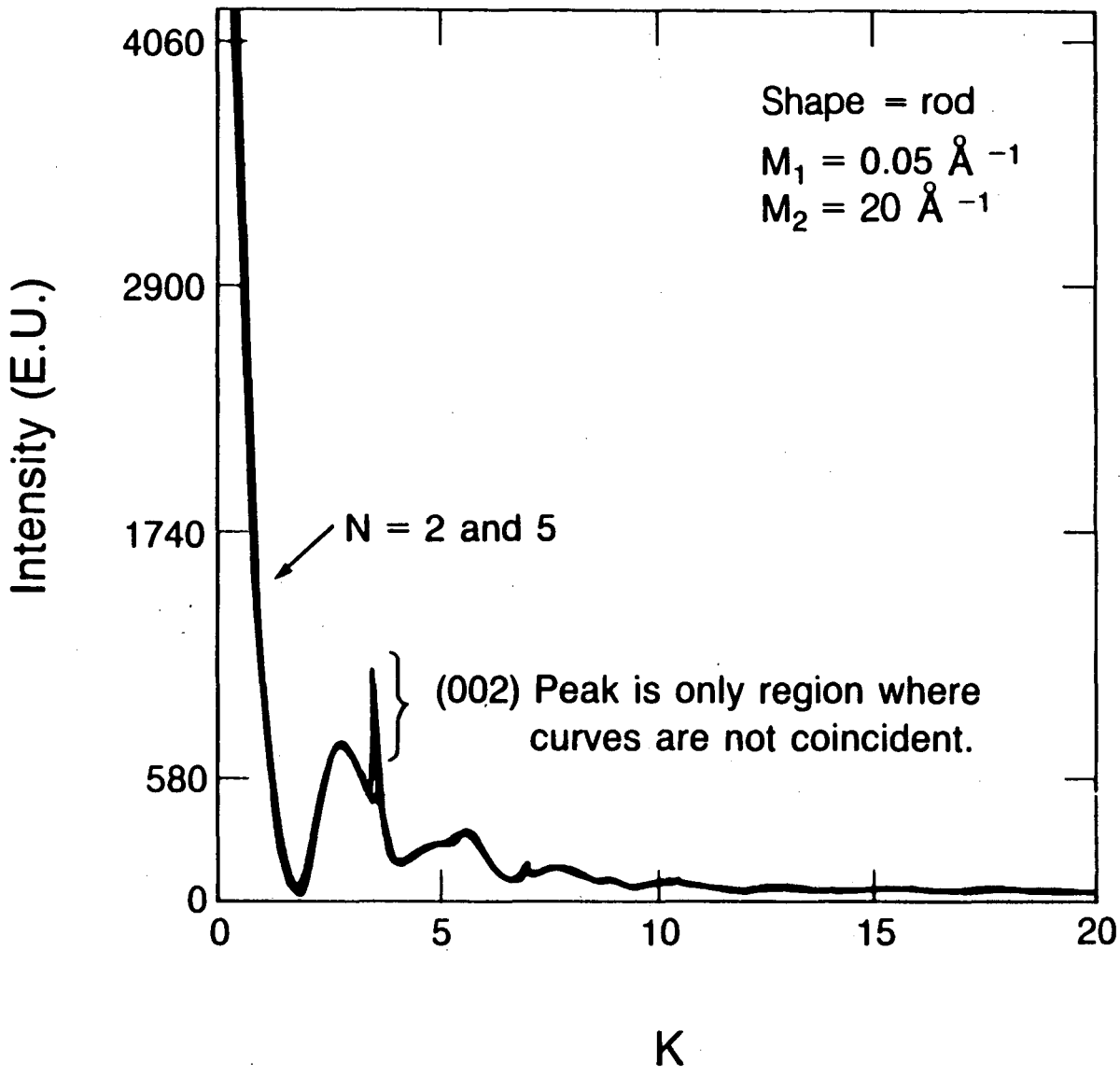

Figure 6c

XBL 844-10424

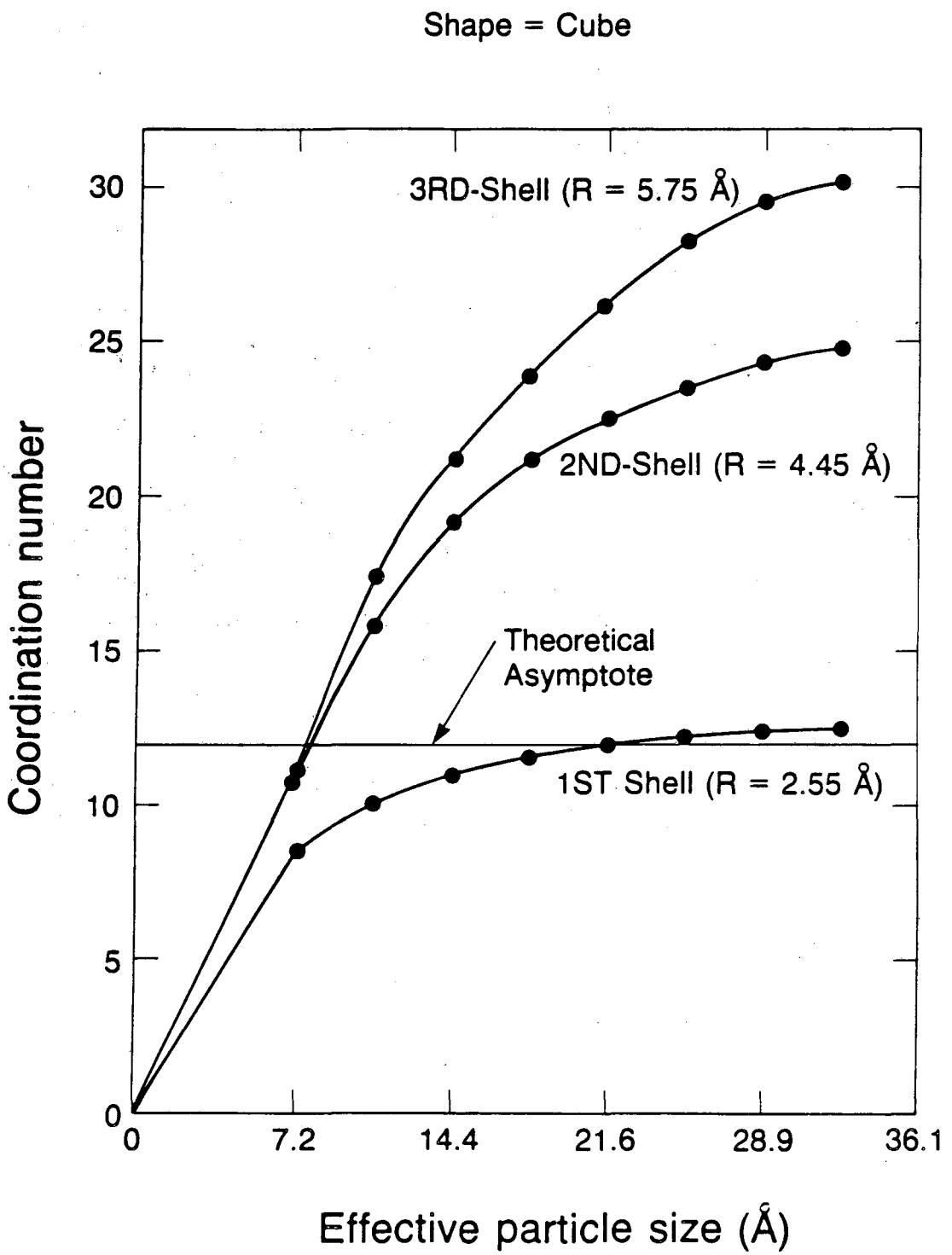

XBL 844-10421

Figure 7

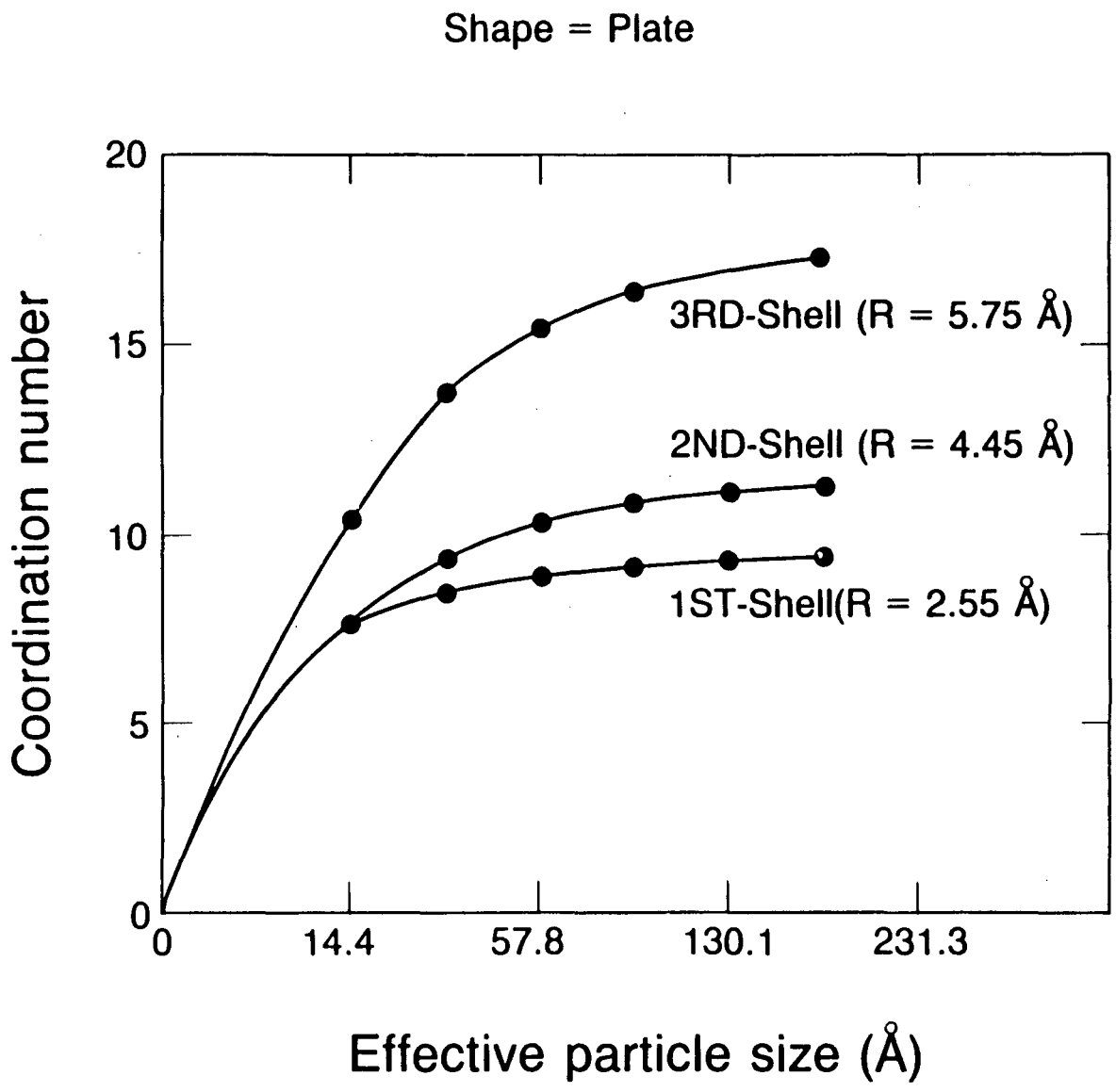

XBL 844-10420

Figure 8

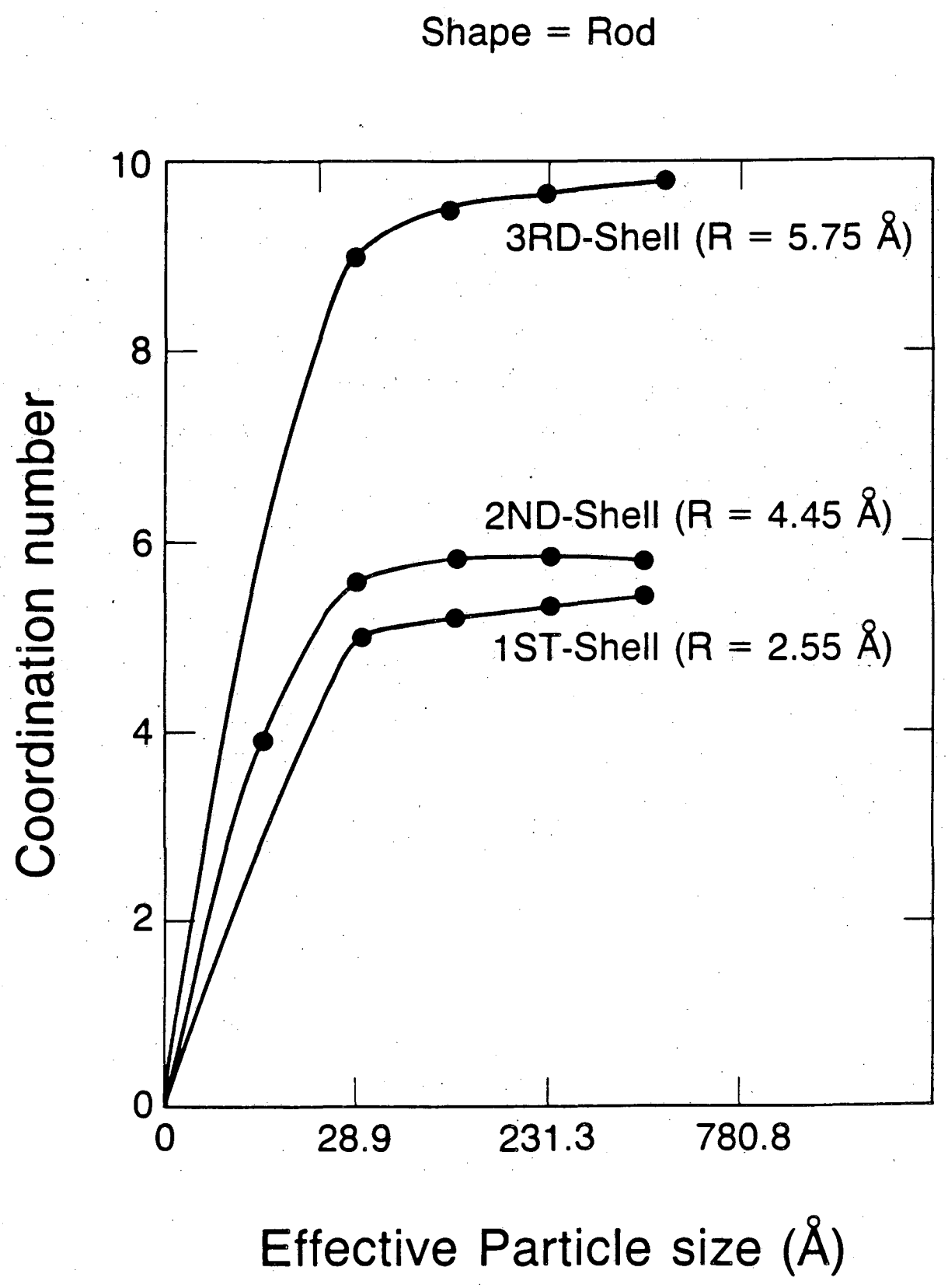

Figure 9

XBL 844-10422

APPENDIX A

VECTORED ARRAY ACCESS

Consider a usual 3-level nested "Do Loop" with variables I,J,K.

```
      Count = 1

      Do      100     I = 1,N
      Do      200     J = 1,N
      Do      300     K = 1,N
      X(Count) =      (I-1)*a
      Y(Count) =      (J-1)*a
      Z(Count) =      (K-1)*a
      Count = Count + 1
300   Continue
200   Continue
100   Continue
```

Rewriting this scheme in terms of vectored access gives:

```
            Count = 1
      Do    100     I = 1,N
       Rim    =     (I-1)*a
      Do    200     J = 1,N
       Rjm    =     (J-1)*a
      Do    300     K = 1,N
      X(Count) =    Rim
      Y(Count) =    Rjm
      Z(Count) =    (K-1)*A
300   Continue
200   Continue
100   Continue
```

When N is large the savings in computation will be substantial since the quantity (Rim) and (Rjm) will be calculated N, and N^2 times respectively instead of N^3 times. Only the most advanced compilers are capable of generating code such as the above from the starting code previously shown.

REVERSAL OF SUMMATION AND MULTIPLICATION CONVERSION

The Debye summation found in this program could be performed as a (3-level) nested "Do Loop" as shown below. The order of the summation can be an important factor in consumption of time as well as possibly providing elimination of other unnecessary loops.

```
Do      50      I1 =1, KMAX3
Do      100     I  = 1, 4N-1
Do      200     J  = I+1, 4N3
        K = I1*.05
```

$$R_{IJ} = X(I)-X(J)^2 + Y(I)-Y(J)^2 + Z(I)-Z(J)^2$$

$$Sum = Sin\frac{KR_{IJ}}{KR_{IJ}} + Sum$$

```
200     Continue
100     Continue
```

$$I.E.U(I1) = Sum\ f^2_{(I1)} + 4M^3\ f^2_{(I1)}$$

```
Sum = 0
50      Continue
```

Instead this summation could be rewritten as:

```
Do      100     I = 1, 4N3-1
Do      200     J = I+1, 4N3
```

$$R_{IJ} = X(I)-X(J)^2 + Y(I)-Y(J)^2 + Z(I)-Z(J)^2$$

Converts division → to multiplication

$$RD_{IJ} = 1/R_{IJ}$$

```
Do      300     I1 = 1, KMAX
```

$$Sum(I1) = RD_{IK}\ Sin(KR_{IJ}) + Sum(I1)$$

```
300     Continue
200     Continue
100     Continue

Do      500     Q = 1, KMAX
```

Division by K → is performed here

$$IEU(Q) = \frac{f^2(Q)Sum(Q)}{K} + 4N^3f^2(Q)$$

500 Continue

The time savings is realized by changing the order of summation and utilizing the reciprocal of R_{IJ}. Similarly the reciprocal of K could have been used to change the line above line 500.

NORMALIZATION OF VARIABLES

One of the most time consuming steps in the program is the generation of coordinates. By normalizing these coordinates by the factor (a/4) where a is the lattice constant much time can be saved.

```
                    Count = 1
                    Do      100     I = 1, 4N^3, 4
                    Do      200     J = 1, 4N^3, 4
                    Do      300     K = 1, 4N^3, 4
These          →    X(Count) =      (I-1)
are the normalized  Y(Count) =      (J-1)
coordinates         Z(Count) =      (K-1)
                    Count = Count + 1
                300     Continue
                200     Continue
                100     Continue
              Do        600     N = 1, KMAX
produces a     →    KDUM(N)   = .05 a / 4
modified K
which converts      K(N)    = .05N actual K in reciprocal space
the normalized    600 Continue
coordinates to real-coordinates
```

TECHNICAL INFORMATION DEPARTMENT
LAWRENCE BERKELEY LABORATORY
UNIVERSITY OF CALIFORNIA
BERKELEY, CALIFORNIA 94720